ADHESIVE WEAR BEHAVIOUR OF ULTRA HIGH STRENGTH BAINITIC STEEL

A DISSERTATION

Submitted in fulfillment of the

requirements for the award of the degree

of

MASTER OF TECHNOLOGY

in

METALLURGICAL AND MATERIALS ENGINEERING

(with specialization in Industrial Metallurgy)

by

GANDHI YASHKUMAR ATULKUMAR

DEPARTMENT OF METALLURGICAL AND MATERIALS ENGINEERING

INDIAN INSTITUTE OF TECHNOLOGY ROORKEE

ROORKEE - 247667 (INDIA)

MAY, 2018

INDIAN INSTITUTE OF TECHNOLOGY ROORKEE

ROORKEE

CANDIDATE'S DECLARATION

I hereby declare that the work carried out in this dissertation entitled, **"Adhesive Wear Behaviour of Ultra High Strength Bainitic Steel"** is presented on behalf of fulfillment of the requirement for the award of the degree of **Master of Technology** with specialization in **Industrial Metallurgy** submitted to the **Department of Metallurgical and Materials Engineering, Indian Institute of Technology Roorkee, India,** under the supervision and guidance of **Dr. Sourav Das,** Assistant Professor, MMED, IIT Roorkee, India.

This is my own work and the results embodied in this thesis have not been submitted to any other institute or university for the award of any degree. The information provided is correct to the best of my knowledge and belief.

Date : /05/2018
Place : Roorkee

Gandhi Yashkumar Atulkumar
M.Tech (Industrial Metallurgy)
Enrollment No: 16544006

CERTIFICATION

This is to certify that the above statement made by the candidate is correct to the best of my knowledge and belief.

Date : /05/2018
Place : Roorkee

Dr. Sourav Das
Assistant Professor,
MMED, IIT Roorkee
Uttarakhand-247667, India

ACKNOWLEDGEMENTS

I would like to express my special gratitude to my supervisor Dr. Sourav Das, for providing me an opportunity to work in this interesting field and guiding me with unceasing advice, encouragement and support. His enthusiasm and strong motivation helps me to solve different problems during my work. He is a great mentor to me. Without his generous help, I could not have accomplished my thesis work. I am truly grateful and proud that I have worked with him. I would like to thank Dr. S K Nath, for allowing me to use Pin on Disc tribometer and profilometer. I would like to acknowledge Mr. Suruj Protim Neog, Research scholar, Indian Institute of Technology Roorkee for providing his support and guidance to carry out the work. I also thank Mr. Nilesh Paraye, Research scholar for conducting my X-ray diffraction tests. I would like to thank my parents and friends to constantly supporting me and motivating me to carry out my work for this thesis.

TABLE OF CONTENTS

LIST OF FIGURES

LIST OF TABLES

ABSTRACT

Ultra high strength bainitic steels have a number of desirable mechanical properties and have been viewed as candidate material for engineering applications. In the current work, an effort has been made to determine adhesive wear behaviour of ultra high strength bainitic steel. The wear tests were carried out on a pin-on-disc tribometer to study the behaviour of nano-structured carbide free bainitic steel. The sliding speed was 1 m/s for all the tests and normal loads of 10 N, 20 N and 30 N were used. The wear resistance was related to mass loss measured after the tests and that helped to determine specific wear rate of the material. Worn surfaces were characterized by using optical microscopy, scanning electron microscopy and atomic force microscopy. Surface roughness was also obtained to familiarize the surface profile of samples after test. Nano-indentation hardness was also obtained in order to analyze the strain hardening effects beneath the contact surfaces. X-ray diffraction (XRD) technique was used to quantify if there is transformation of any phases under high mechanical loading during wear and to analyse effect of loading on different parameters like strain, dislocation density and crystallite size.

Chapter 1

INTRODUCTION

Wear is progressive damage, involving material loss, occurs on the surface as a result of relative motion between the surfaces. In most of the practical applications sliding surfaces are lubricated in some way, and the wear that occurs is termed as lubricated sliding wear. In some engineering applications and mainly in laboratory investigations, surfaces slides in a air without any lubricant, and the wear that occurs is termed as dry sliding wear.

There are different types of wear which is classified based on the mechanism of wear.

1) Abrasive wear
2) Surface fatigue wear
3) Erosive wear
4) Adhesive wear

In, Abrasive wear hard particles between two sliding surface contribute to the wear mechanism [1]. Polishing of samples with the help of emery papers is the most practical example of abrasive wear. Abrasive wear commonly observed in mainly all earth moving equipments like excavators, skid-steer loaders, etc.

Surface fatigue wear is observed during the repetitive action a fluctuating load. These repeated loading and unloading cycles may induce formation of surface or subsurface cracks. These cracks result in chunks of material being removed from the surface. It is commonly observed in ball bearing, roller bearing, etc.

Erosive wear is similar to the adhesive wear but here the hard particles attacks the adjacent material with very high velocity. Erosive wear commonly observed in propeller blades of ships, blades of turbine, blades of helicopter.

Adhesive wear, is the wear due to localized bonding (Micro-weld formation) between contacting solid surfaces and that leads to material transfer between the two surfaces or the loss from either surface. The adhesive wear is also known as sliding wear either in the presence or absence of lubricant. Adhesive wear commonly observed in the sliders, bearings, gears, rail tracks, etc.

In this study, focus is made on adhesive wear behaviour of ultra high strength bainitic steel, which was developed by Das and Haldar [2]. The objective is to provide an increased understanding of tribological behaviour of ultra high strength bainitic steel in order to contribute to the on-going work of discovering its possible applications. Therefore, since this ultra high strength bainitic steel present good combination of mechanical properties (Strength-elongation); it may find its use in a wide variety of application such as automotive, rail industries, etc [3].

Chapter 2

LITERATURE REVIEW

2.1 Mechanism of adhesive wear

A typical adhesive wear system consists of the two bodies, which are in contact either in presence or absence of lubricant. There is always presence of surface irregularities on the surface of body. Initially when two bodies are in contact, asperity contact is less. That indicates that there is low area of contact so, stress generated is high. If this magnitude of stress is higher than Yield strength (σ_y) of the material, then deformation occurs at the asperity contact and diffusion of mass can be observed. Due to this phenomenon solid state bond (Micro-weld formation) is generated at the contact. Now, when two surfaces slide over each other with application of load, micro weld bonds get broken and the particles coming out is known as wear debris.

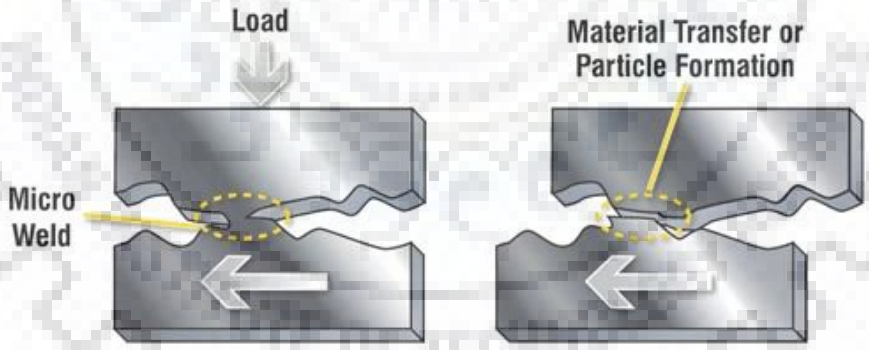

Figure 2.1: Schematic of mechanism of adhesive wear

2.2 Adhesive wear and its economic importance

Adhesive wear is relatively slower and accounts for 30-45% of material loss over all possible wear scenarios [Table2.1]. It is commonly observed in piston-cylinder of I.C engine, bearing, gears, rail tracks (Fig.2.2), etc.

Table 2.1: Relative importance of the types of wear

Type of Wear	Eyre(1976)[4]	Rabinowicz(1983)[5]
Adhesive Wear	23%	45%
Abrasive Wear	58%	36%
Erosive Wear	5%	4%
Surface Fatigue Wear	14%	15%

Figure 2.2: Practical application of adhesive wear phenomena in rail tracks

2.3 Theory of adhesive wear

Assumptions:

- All the contacting asperities are of spherical shapes with the same radius.
- The contact between two surfaces occurs where asperities are in contact, so the true area of contact is equal to the sum of the area of contact of each individual asperity.
- This area is closely proportional to the normal load and it can be assumed that for metals, local deformation of asperities will be plastic.

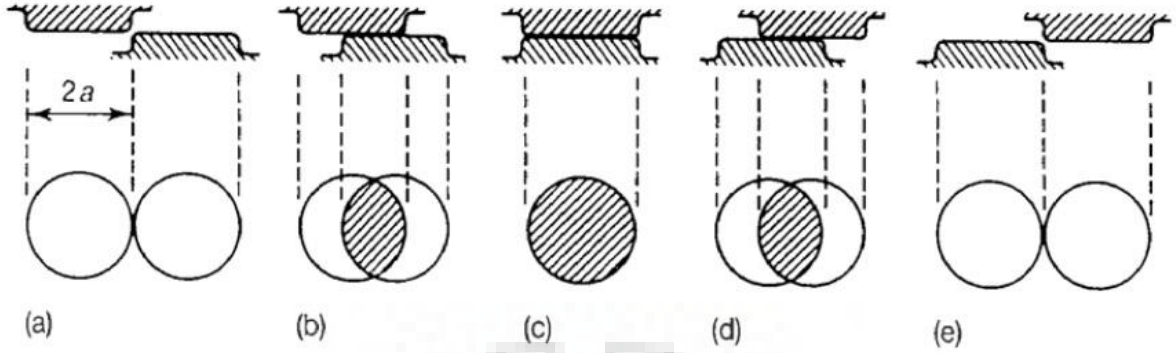

Figure 2.3: Schematic diagram showing the evolution of a single contact patch as two asperities move each other [1]

In the Fig.2.3(C) Asperity contact has reached maximum size, and the normal load supported by it can be given by,

$$\delta W = P\pi a^2$$

Here,

P = yield pressure for the plastically deforming asperity (which is close to its hardness H),

δW = Normal load acting on one asperity,

a = Radius of the spherical asperity,

Now,

Total load (W) = $\sum \delta W = \sum P\pi a^2$

Now, when micro-weld is broken and asperity contact reached to the zero as shown in the Fig.2.3(e) , some amount of wear volume is come out and that can be given by,

$$\delta V = \frac{1}{2}\left(\frac{4}{3}\pi a^3\right)$$

$$\delta V = \left(\frac{2}{3}\pi a^3\right)$$

Now, Wear rate can be given by,

Wear rate $\left(\frac{V}{S}\right) = \frac{Wear\ volume}{Sliding\ distance}$

Wear rate for one asperity contact can be given by,

$$\frac{V}{S} = \frac{\delta V}{2a}$$

$$\frac{V}{S} = \frac{\pi a^2}{3}$$

Now, it is not possible that all the asperities contact give rise to wear particles, let us assume that only some proportion k is the amount,

$$\frac{V}{S} = k\,\frac{\pi a^2}{3}$$

Total wear rate for all asperities contact can be given by,

$$\frac{V}{S} = \frac{k}{3}\sum \pi a^2$$

$$\frac{V}{S} = \frac{k}{3}\left(\frac{W}{P}\right)$$

$$\frac{V}{S} = K\left(\frac{W}{H}\right)$$

Here,

K = $\frac{k}{3}$ = Archard wear co-efficient,

P = H(Hardness of material), [kgf/mm^2],

V = Wear volume, [mm^3],

S = Sliding distance, [mm].

2.4 Literature review on Rolling/Sliding wear

Early research work on the rolling/sliding wear of bainitic steels started with the comparison of wear rates between pearlitic steels and bainitic steels. Aim was to replace pearlitic steels by much stronger bainitic steels used in the rails applications [6-11]. Observations were not straightforward, as in certain cases, bainitic steels exhibited lesser

wear resistance compare to pearlitic steels. Here, showing some of the detailed research studies on that comment.

Jose velez et.al [12] investigated experiment on pin-on-disc tribometer for AISI 1070 pearlitic steel and AISI 15B30 bainitic steel pin samples, sliding against AISI 1085 pearlitic steel disc. The sliding speed was kept 1 m/s and Normal loads of 10, 30 & 50N were used. Composition of materials used is given in the Table 2.2.

Table 2.2: Compositions of materials in Weight Percentage [12]

Steel	C	Mn	P	S	Fe
AISI 15B30	0.35	1.5	0.26	0.02	Balance
AISI 1070	0.65-0.75	0.6-0.9	0.04	0.05	Balance
AISI 1085	0.8-0.94	0.7-1	0.04	0.05	Balance

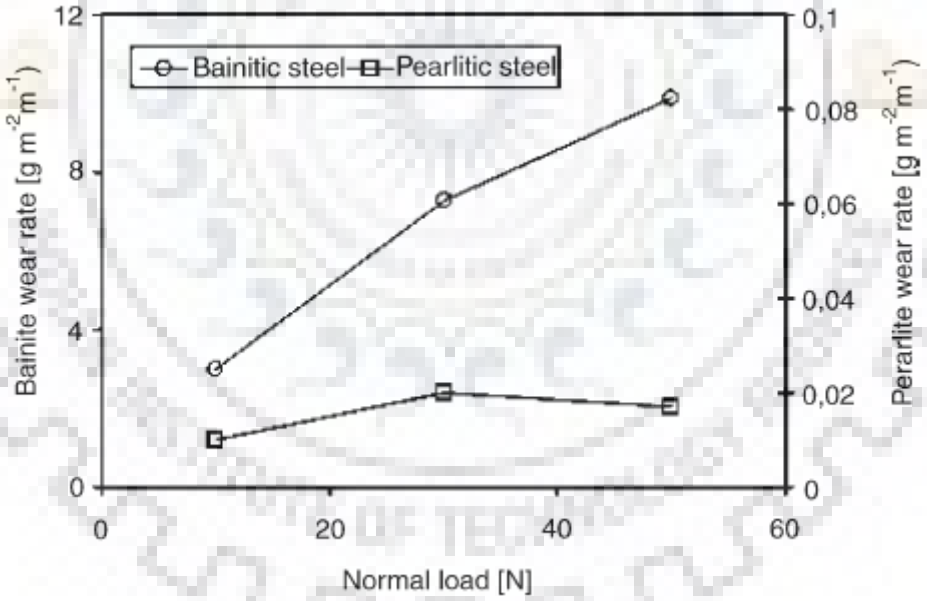

Figure 2.4: Wear rate against Normal load for Pearlitic & bainitic steels [12]

The results shows that in AISI 1070 pearlitic steel wear rates were low and the surfaces remains relatively smooth. The reason for that may be due to the shape and distributions of carbides, which can be represented by inter-lamellar spacing in pearlitic steel; and higher carbon percentage also contributed to the higher wear resistance in AISI 1070 pearlitic steel. But, in case of AISI 15B30 bainitic steel adhesive wear effects were much

more prominent, mainly due to the intense plastic deformation and the poor strain hardening of microstructure. In that steel, mass losses were three orders of magnitude higher than in AISI 1070 pearlitic steel and surfaces were found to be more rough [12].

This fact was considered true until Clayton and other challenged previous research with organized studies on sliding wear of a series of bainitic alloys [13-19]. Still it is difficult to make direct comparison but Table 2.3 shows the wear rates of a few alloys with various microstructure and hardness. Jin & Clayton made an effort to compare the sliding/rolling wear rate of pearlitic and bainitic steels. It is interesting to note that wear rate of pearlitic steels strongly depend on the bulk hardness, where as the hardness has a very less influence in case of bainitic steels [11,18] (Fig. 2.5). In case of pearlitic steels, it is found that wear resistance increases with increasing hardness and that is possible by decreasing inter-lamellar spacing [13,18]. Now, in case of bainitic steels, material with good impact toughness can offer wear resistance that same of pearlitic steels [15].

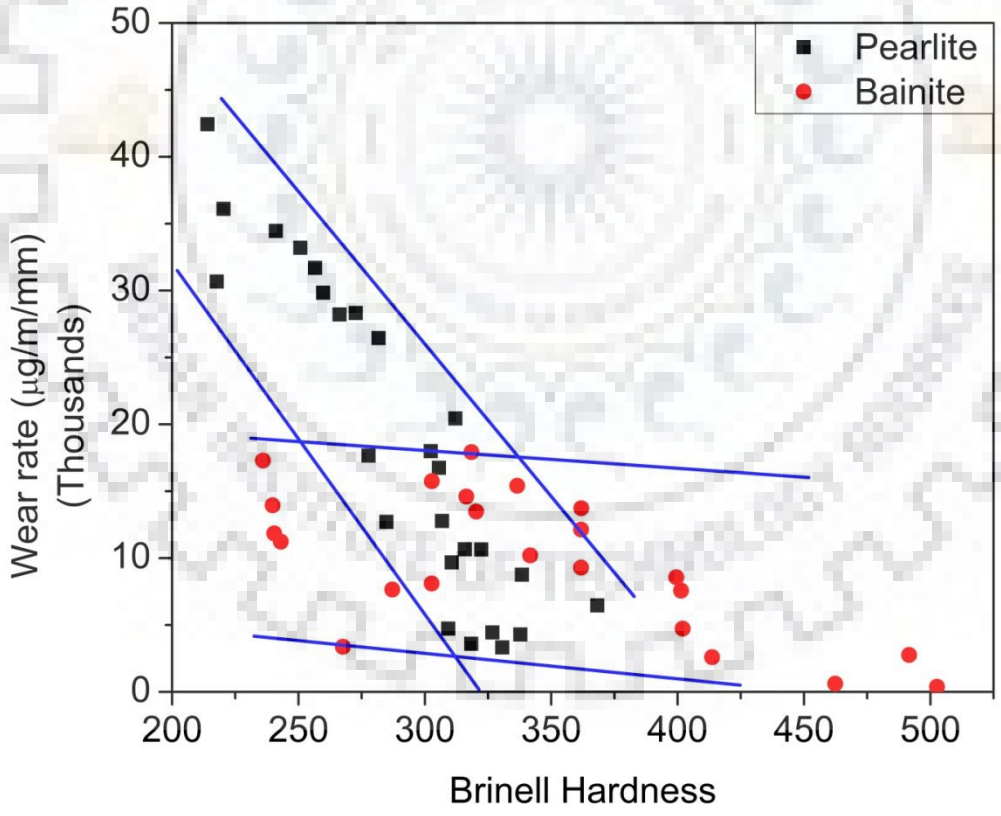

Figure 2.5: Wear rate of pearlitic and bainitic steels over a wide range of hardness [18]

Table 2.3: Comparison of rolling/sliding wear rate of various structures and hardness

Alloy	Hardness	Microstructure	Wear rate	Reference
0.18C-2.01Mn-1.94Cr-0.48Mo-0.0027B	40 HRC	Carbide-free bainite	13.5×10^{-6} g m^{-1} mm^{-1}	[11]
0.11C-3.97Mn-0.017Cr-0.47Mo-0.0027B	35 HRC	Lower bainite	17×10^{-6} g m^{-1} mm^{-1}	[11]
0.08C-2.03Mn-1.97Cr-1.93Ni-0.47Mo-0.0031B	35 HRC	Granular bainite	16×10^{-6} g m^{-1} mm^{-1}	[11]
0.026C-4.04Mn-0.018Cr-0.019Ni-0.47Mo-0.0030B	36 HRC	Carbide-free lathe ferrite + massive ferrite	17×10^{-6} g m^{-1} mm^{-1}	[11]
0.04C-0.08Mn-0.19Si-2.76Cr-1.93Ni-0.25Mo-0.0023B	223 HRB	Bainite	8×10^{-3} g m^{-1} mm^{-1}	[18]
0.11C-0.57Mn-0.19Si-1.68Cr-4.09Ni-0.58Mo-0.0023B	293 HRB	Bainite	8.4×10^{-3} g m^{-1} mm^{-1}	[18]
0.45C-2.08Si-2.69Mn	HV 484	Bainite(329ºC)	1×10^{-13} m^3 mm^{-1}	[20]
0.45C-2.08Si-2.69Mn	HV 423	Bainite(382ºC)	1.1×10^{-13} m^3 mm^{-1}	[20]
0.45C-2.08Si-2.69Mn	HV 590	Bainite(422ºC)	0.25×10^{-12} m^3 mm^{-1}	[20]
0.45C-2.08Si-2.69Mn	HV 760	Martensite	0.50×10^{-12} m^3 mm^{-1}	[20]
0.45C-2.08Si-2.69Mn	HV 531	Tempered Martensite	0.24×10^{-12} m^3 mm^{-1}	[20]
0.45C-2.08Si-2.69Mn	HV 320	Normalized	0.2×10^{-12} m^3 mm^{-1}	[20]

Wear properties may vary due to amount of elements present in the steels. Earlier Clayton was working on low carbon steels. But he has also worked on the high carbon alloying steels. Clayton et.al [16] investigated experiment on the Amsler wear testing machine. The materials used for the research was three different compositions of bainitic steels & pearlitic steels with carbon percentage of 0.04, 0.10 and 0.52 wt%. Pearlitic steel with 0.70 wt% C was used as the counter disc material. The load applied to the rollers was

between 300 N to 2000 N that can generate maximum contact pressure of 500 to1220 N/mm^2 respectively. As we have seen that steels with bainitic microstructure offers the good high strength and toughness, an almost incompatible combination of pearlitic steels.

The suitability of bainitic steels for wheel and rail applications has been discussed in a number of previous investigations [21-23]. However, none of the studies were done on systematic investigation of bainitic steels and pearlitic steels with respect to test conditions, chemical compositions and mechanical properties. The result indicates that the wear rate for three bainitic steels fall within the band of pearlitic steels [11,12].

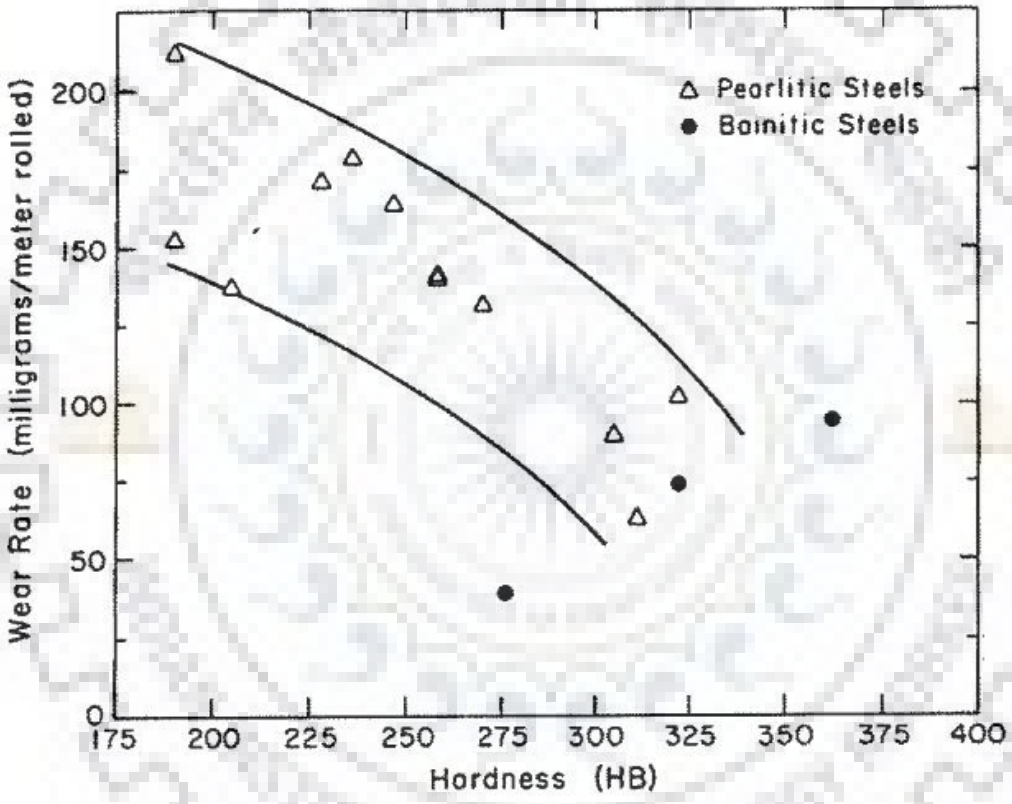

Figure 2.6: Plot showing effect of hardness on wear rate for bainitic & Eutectoid pearlitic steels [16]

The research shows that in case of pearlitic steel with increases in the hardness, the wear rate reduces, where as in case of bainitic steel with increase in the hardness, wear rate increases. The results shows that in case of bainitic steel, sample with 0.52% C shows the lower wear resistance than pearlitic steel of same hardness and sample with 0.04% C shows the good wear resistance compare to pearlitic steel of same hardness (Fig. 2.6). The reason for that can be understood by following explanations. With increase in the hardness of pearlitic steel, the inter lamellar spacing of pearlite is reduced. That leads to work hardening

and it offers good wear resistance. Sufficient amount of Si (0.25 to 0.27 wt%) in the bainitic steel will lead to formation of higher amount of austenite phases and retard the formation of cementite. More amounts of austenite phases contribute to the strain hardening of material. So, here bainitic steels offers good wear resistance compared to pearlitic steels and it is completely opposite to the other investigation in which Si content was very low[12]. The resistance of bainitic steels to type III wear is influenced by the strain resistance. The results indicate that bainitic steels achieved surface Knoop hardness 507 HK compared to 402 HK of pearlitic steels for the same initial bulk hardness of 28 HRC [16].

Chattopadhyay et. al [24] performed the experiment on the ball on plate reciprocatory sliding wear test machine. Here, two microalloyed steels of different composition were used. These steels were isothermally annealed to get pearlitic and bainitc microstructure. A hardened steel ball of average hardness of 800 VHN was used as a counter material. The specimens were tested for normal load of 20 N to 50 N and frequency from 5 to 11 Hz.

Table 2.4: Compositions of steels(weight percentage)[24]

Steel	C	Mn	Si	V	Cr	Ni	Mo	P	S	Al	Cu
SM1	0.51	0.88	0.5	0.1	0.15	0.009	0.015	0.016	0.019	0.074	0.02
SM2	0.42	0.93	0.29	0.1	0.19	0.024	0.016	0.017	0.019	0.077	0.022

Here, the wear data of the test is shown in the following Fig.2.7 (a) and 2.7 (b).

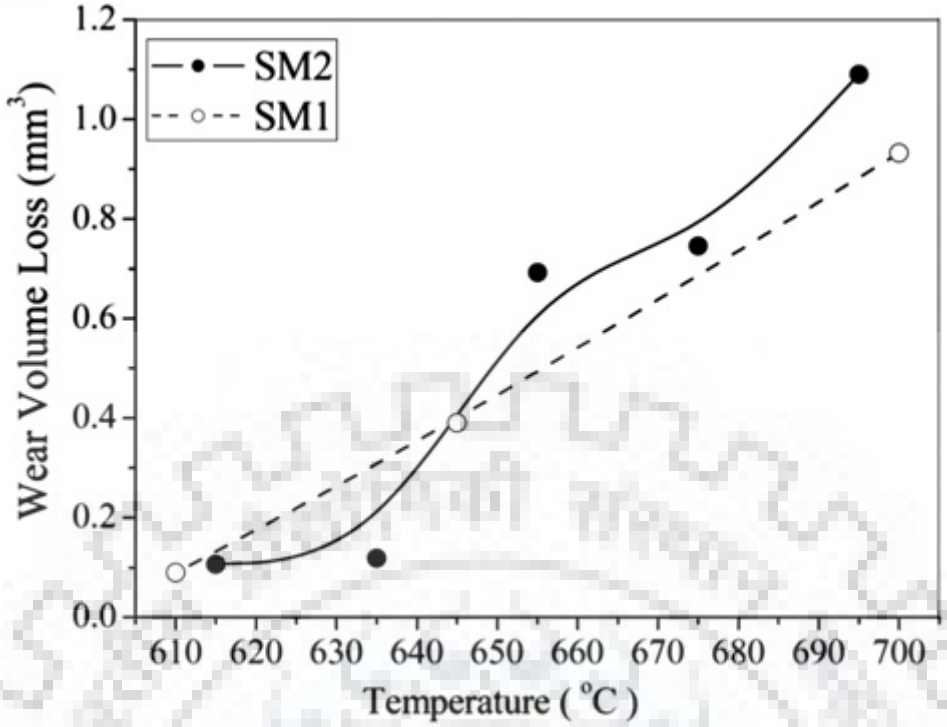

(a)

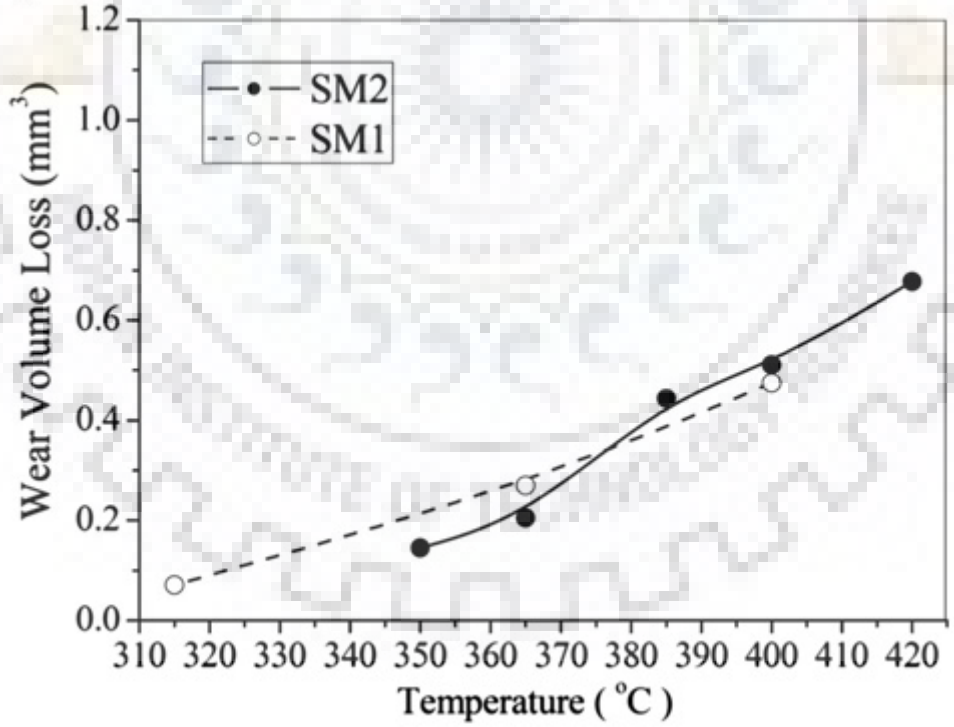

(b)

Figure 2.7: Wear volume loss against isothermal heat treatment temperature for the steel samples in (a) pearlitic (b) bainitic condition [24]

The results show that bainitic steel samples of both compositions follows the same trend as pearlitic steels but with very low wear volume loss. So, the bainitic steels offers superior wear resistance compare to pearlitic steels for the same composition. This is attributed to the intergranular wear for pearlitic steels and intragranular wear for bainitic steels. As the isothermal treatment temperature increases hardness of the material decreases [25]. So that material becomes soft and ductile, that leads to higher wear volume loss.

Carbide-free bainitic steels with fine bainitic ferrite laths separated by the films of high-C austenite show good wear resistance [26-28], compared to structures of equivalent or more hardness [29-31]. The refined structure imparts a high hardness and toughness with the austenite retarding crack propagation and that leads to reduction of wear. In all these cases, a hard thin friction layer of extremely fine ferrite grains is found at the wear surface, which is forming due to transformation of austenite to martensite caused by surface shear strains due to sliding. The wear resistance was found to increase due to the reasons mentioned above [28].

2.5 Problem Formulation

Qualitative observations indicate that the bainitic steels subjected to rolling/sliding condition does not perform well compare to pearlitic steels with similar hardness and loading conditions. But the nanostructure carbide free bainitic steels offers a good performance under rolling/sliding compare to pearlitic and bainitic steels. Nanostructure carbide free bainitic steels consisting of fine plates of bainitic ferrite embedded in carbon-enriched retained austenite. In this research also the material that is going to be used is nanostructure carbide free bainitic steel, which is having excellent strength-elongation property. To understand the material performance under the application of adhesive wear the following research is carried out. In this work, an effort has been made to get a deeper understanding of the dry sliding wear resistance of nanostructure and ultra high strength bainitic steel, using high-resolution characterisation methods. Specific wear rate of the material is determined to compare with other commercially available carbide free bainitic steel for the use of practical application.

2.6 Plan of work

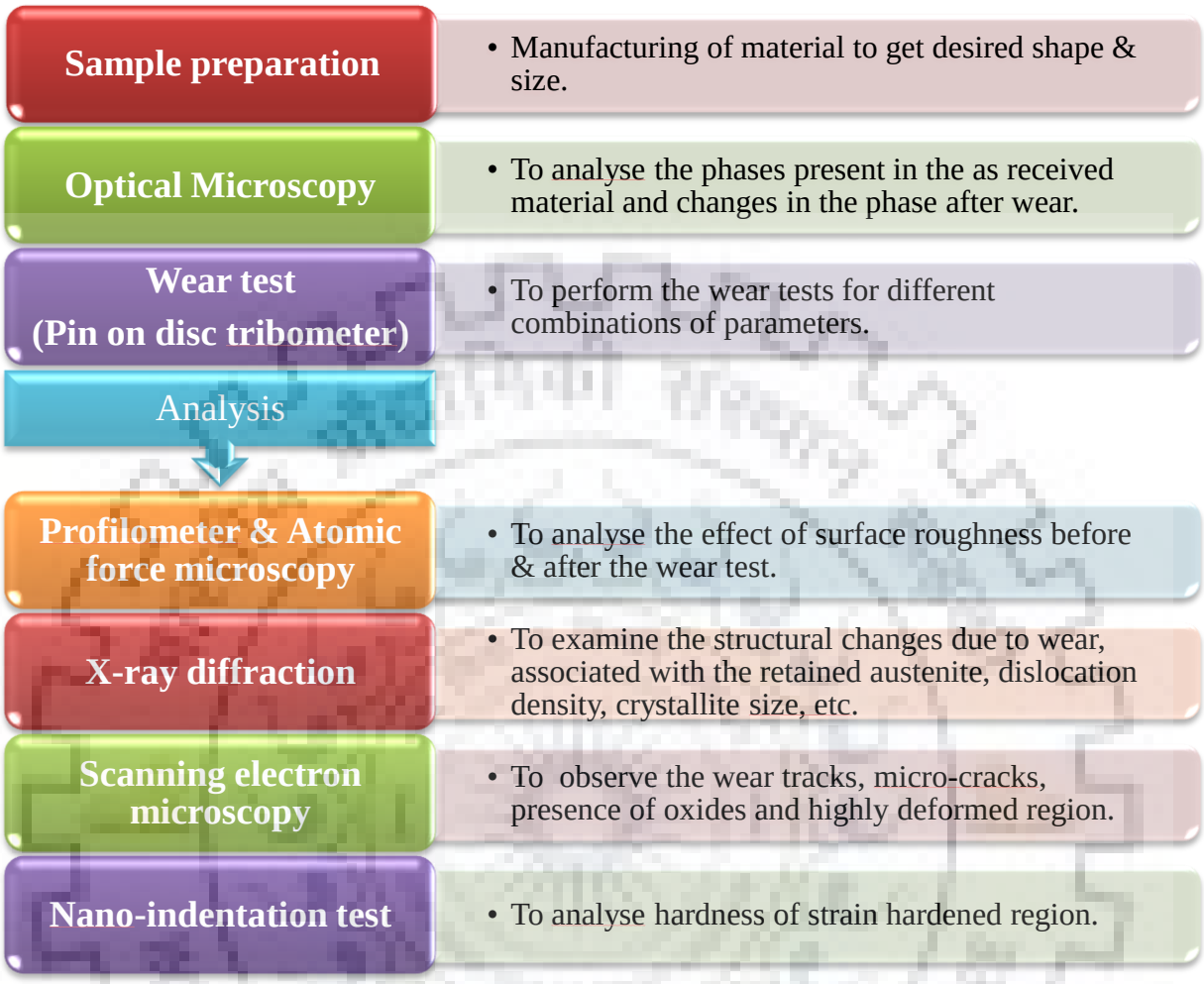

Chapter 3

EXPERIMENTAL PROCEDURES

This chapter gives a complete overview of the experimental techniques adopted for the research. It includes detailed understanding of Introduction of testing materials, Wear testing instrument, Metallography, Surface roughness measurements, Nanoindentation testing and X-ray diffraction.

3.1 Introduction of the material

The steel was produced as a part of important work on the continuously cooled ultrafine bainitic steel with excellent strength-elongation combination for commercial engineering applications by Das and Haldar [2] in TATA steel. Main intention was to design such steel that can be produced in any hot strip mill, after accelerated cooling on the runout table followed by cooling. The chemical composition of the material is listed in the following Table 3.1. In this steel, silicon was added to prevent the precipitation of hard phase cementite during the bainitic transformation. Manganese and chromium enhance hardenability. Aluminium and titanium help in accelerating the transformation.

Table 3.1: The chemical composition of the material

Elements	**C**	**Mn**	**Si**	**Cr**	**Al**	**Ti**
Weight%	0.34	1.80	1.51	0.92	0.015	0.032

This steel shows excellent strength-elongation properties which can be easily observed by its stress-strain diagram (Fig.3.1). Overall mechanical properties of the material are shown in the following Table.3.2.

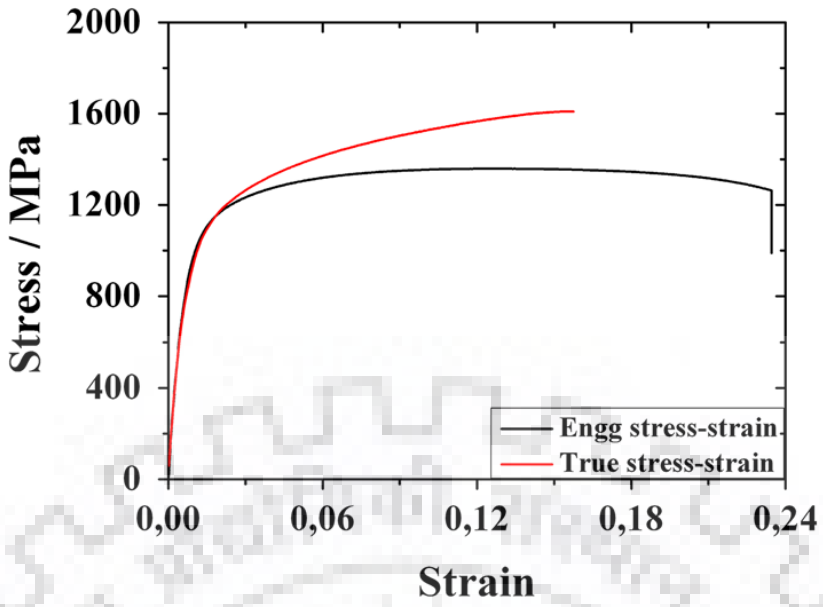

Figure 3.1: Engineering and true stress-strain curve of carbide-free bainitic steel sample[2]

Table 3.2: Mechanical properties of the material[2]

YS (MPa)	UTS (MPa)	Uniform Elongation (Percentage)	Total Elongation (Percentage)	Hardness (VHN)
980±25	1385±15	13.6±0.5	22±1	413±9

3.1.2 Sample preparation

The steel material was in the shape of square plate as shown in the Fig.3.2. The samples for were tests were machined out from the square plate. The thickness of this as received plate was 3 mm. The machining processes were done under control conditions so that generation of additional residual stresses due to cold work can be avoided. As per the availability of tribometer instrument, samples (pins) were made up of cylindrical shape having diameter of 6 mm and thickness of 3 mm as shown in the Fig.3.3.

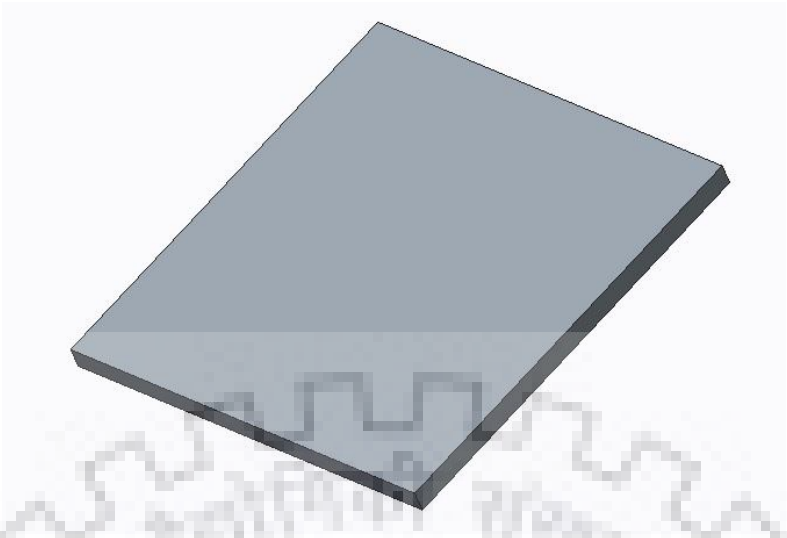

Figure 3.2: Schematic of the steel material in as-received condition

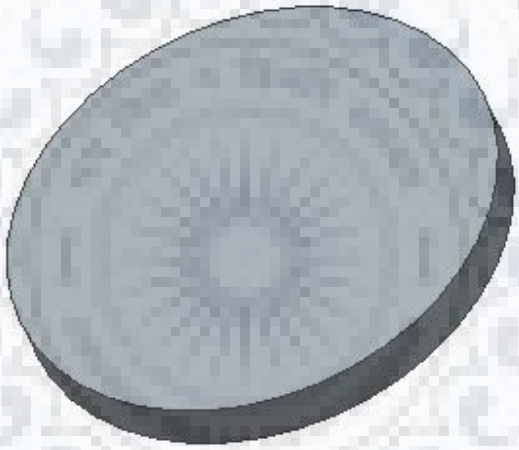

Figure 3.3: Schematic of the test specimen (pin sample)

3.2 Wear testing instrument

Pin on Disc tirbometer was used to perform the experiments as shown in the Fig.3.4. The standard test method G99 was followed for wear testing of all samples. To execute the experiments, a pin with a circular surface tip is positioned perpendicular against flat circular counter disc. The material of disc is EN 31. The disc used is of standard size, having diameter of 165 mm and thickness of 8 mm. The hardness of disc is 58-60 HRC, which is equivalent to 690-740 VHN. The chemical composition of disc is shown in the Table 3.3.

Figure 3.4: Pin on disc tribometer used to perform wear testing

Table 3.3: The chemical composition of counter disc material

Element	C	Mn	Si	Cr	Others
Weight%	1.00	0.50	0.20	1.40	Balance

3.2.1 Steps of laboratory experiments

- A pin with circular surface tip (ϕ 6mm × h 3mm) is positioned perpendicular to a flat counter disc. The pin specimen was pressed against the counter disc with the application of different external load like 10N, 20N, etc by the means of lever. Here, it was difficult to hold this smaller cylindrical pin specimen on the tribometer directly, so one sample holder is designed based on the specification of the pin on disc setup (Fig.3.5).
- Before mounting the samples on the sample holder and starting of experiments, disc was polished with 2000 grit size emery paper so that all the foreign particles can be removed. After polishing disc was cleaned with Acetone solution. The pin sample was then inserted in a sample holder.

Figure 3.5: Schematic of sample holder

- Experiments were performed under control parameters conditions. The sliding velocity was kept constant 1 m/s for all the experiments. Track diameter and rpm of counter disc was adjusted such that, it can give sliding velocity of 1 m/s.
- The principle measurable parameters in the experiments were amount of weight loss and frictional force. The specimen was weighed before the starting of experiments and it was also weighed after every time interval of experiments. The frictional force is noted down to calculate co-efficient of friction.
- After stipulated time interval test was stopped and pin samples were removed and cleaned with Acetone solution, so that all the wear debris attached to the pin samples can be removed. Weight loss was measured to calculate specific wear rate of the material.
- To obtain pure adhesive wear mechanism, it was necessary to cleaned wear debris from the counter disc. Otherwise, there may be different wear mechanism took place like three body abrasion. The parameters list shown in the following Table 3.4.

Table 3.4: Pin on disc test parameters

Normal load	10 N, 20 N, 30 N
Sliding velocity	1 m/s
Time intervals	15 + 15 + 15 + 30 + 90 + 150 minute
RPM of disc	Track diameter was adjusted in a such way that it can give sliding velocity of 1 m/s $\left(V = \frac{\pi DN}{60}\right)$

3.3 Microstructural characterization

3.3.1 Sample preparation

Metallographic sample preparation of pin samples requires special care, as surface roughness can highly influence the adhesive wear phenomena. Each pin samples were polished with up to 2000 grit size silicon carbide emery papers. To make proper contact between pin samples and disc, it was also necessary to have complete flat surface of pin specimen. Polishing was done politely so that generation of additional stresses can be avoided on the tip surface of pin samples.

3.3.2 Optical metallography

Optical microscopy is a technique which is used to study the microstructure and the basic elements present in the sample. A Leica Microsystems Model 5000M light microscope was used for all of the optical microscopy work. All the optical microscopy work was done with the magnification in the range of 100 to 500X. Mostly, bainitic structure is clearly visible at the magnification of 500X. A Leica Application Suite Software, ImageJ was used for minor digital modifications of the micrographs taken like cropping, addition of scale bars, contrast and brightness adjustments.

3.3.3 Scanning electron microscopy

The secondary electron images were taken in a FE-SEM Quanta 200 FEG and Zeiss EVO18 scanning electron microscope, operated under maximum 30 kV acceleration voltage, with maximum probe current of 100 nA and 20 kV gun potential respectively. The working distance was maintained within 8-11 mm for high magnification images (3000X). EDX detector was also used for the chemical analysis of the worn samples.

3.3.4 Surface roughness measurements

The surface roughness was measured using profilometer and atomic force microscope (AFM). Mititoyo SJ 400 profilometer was used to measure overall average surface roughness of specimens before and after the wear test linearly. INTEGRA NT-MDT-INTEGRA atomic probe microscope was used to measure surface roughness of specified area (e.g 50×50 μm) of

samples before and after wear test. AFM provides 3D profile of the surface details. XY direction position resolution and optical resolution of AFM was 5µm and 1 µm respectively. Minimum resolution of profilometer was 0.000125 µm.

3.3.5 Nanoindentation testing

A sharp Berkovich nanoindenter setup was used to perform nanoindentation on the pin samples to know the variation of hardness beneath the top surface after wear. Diamond was used as the indenter having tip radius of 100 nm and 3 face pyramid shape.. Tests were performed under the normal load of 2500 µN. Load was applied at the constant loading rate of 500 µN/sec and dwell time was kept 2 sec at a peak load. The cross-section of pin samples were polished with high grade silicon carbide emery papers and it was mounted on the bakelite material to get desire flatness and shape.

3.3.6 X-ray diffraction

A vertical X-ray diffractometer was used with the scanning mode over a range of 2θ = 45º-130º with a scan step of 1º and dwell time of 1 min per step. The radiation used was CoK_{α} having wavelength (λ = 1.789 Aº). From the X-ray pattern the quantitative phase analysis, crystallite size and strains were also estimated.

Standard strain-free crystals of Si were diffracted in the same instrument over a 2θ range of 30º-120º in order to measure the instrumental broadening of the X-ray diffractometer. The X-ray pattern of Si was analysed in Xpert HighScore+ and appropriate values of instrumental broadening was calculated. X-ray diffraction pattern of strain free pure Si crystals used for calculation of instrumental broadening is shown in the Fig.3.6.

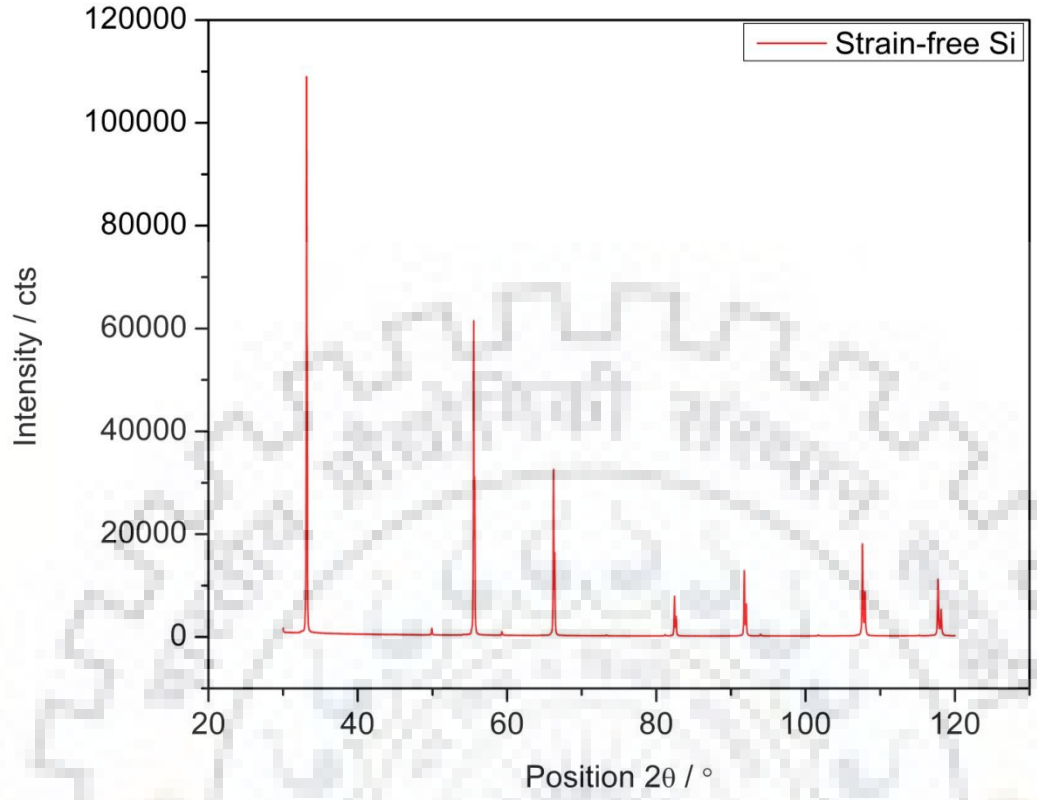

Figure 3.6: X-ray diffraction pattern of strain-free pure Si crystals used for the calculation of instrumental broadening of diffractometer

3.3.7 Williamson-Hall plot

After the peak fitting of the X-ray diffraction pattern of all the samples in Xpert High Score+, some calculations were done to find out crystallite size, dislocation density, strain, etc. the average size of the crystallites (D) can be calculated using Debye-Scherrer's formula,

$$D = \left(\frac{k\lambda}{\beta_c cos\theta}\right)$$

Where,

k = the shape coefficient for the reciprocal lattice point, normally taken as 0.9,

λ = 1.789 A^o, the unfiltered wavelength of the CoK_α radiation,

β_c = Crystallite size broadening.

If the microstrain induced in the crystallites due to imperfections like voids, dislocations, stacking faults are assumed to be uniform in all crystallographic directions, then the microstrain (ε) can be expressed as,

$$\varepsilon = \left(\frac{\beta_s}{4tan\theta}\right)$$

Where, β_s = Strain broadening,

Though the scherrer formula is accurate enough to calculate the crystallite size, in case of adhesive wear, where high strain accumulates near the surface, striping off peak broadening due to lattice microstrain, along with instrumental broadening should results in more accurate calculation.

If the measured peak broadening is expressed as β and instrumental broadening is expressed as β_i, then, for purely Lorentzian profile of the X-ray peak, it can be expressed as,

$$(\beta - \beta_i) = \left(\beta_c + \beta_s\right) = \beta_r$$

$$\beta_r = \frac{k\lambda}{Dcos\theta} + 4\varepsilon\, tan\theta$$

Rearranging above equation as,

$$\beta_{hkl}\, cos\theta = \frac{k\lambda}{D} + 4\varepsilon\, sin\theta$$

These set of equations are known as Williamson-Hall plot equations. For isotropic nature of the size of the coherent domain of diffraction and crystallite microstrain, a $\beta_{hkl}\, cos\theta$ against $sin\theta$ plot should yield a straight line. The slope of the lines gives an estimation of crystallite microstrian and the y-intercept gives the values of crystallite size.

Chapter 4

RESULTS AND DISCUSSION

In this chapter complete results of the different experiments like wear data, surface roughness, coefficient of friction, optical microscopy, scanning electron microscopy, nanoindentation, X-ray diffraction analysis, etc. are explained.

4.1 Wear data

Wear plot is generally expressed as Cumulative volume loss against sliding distance as shown in the Fig. 4.1. It can help to calculate the specific wear rate of the material.

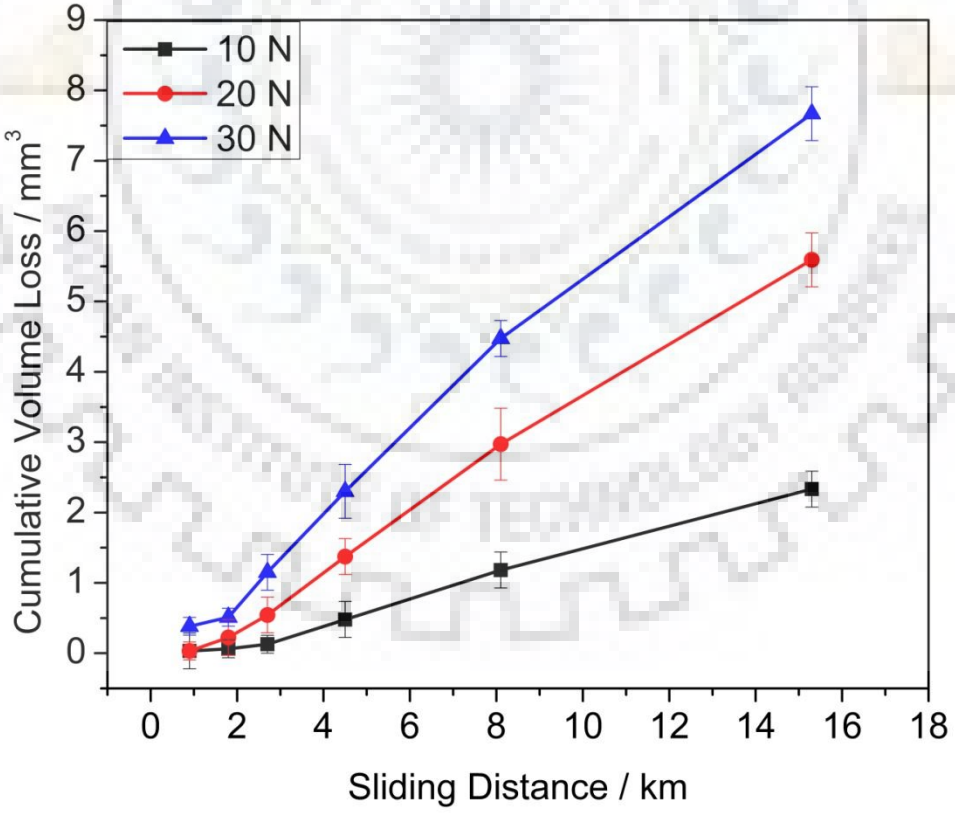

Figure 4.1: Plot of cumulative volume loss from bainitic pin specimens during sliding under the application of 10, 20 and 30 N normal loading condition

The linear nature of the plot indicates that Cumulative volume loss of the material is proportional to sliding distance. The wear test result indicates that application of normal load has direct influence on the cumulative volume loss of the material. Because at higher application of normal load, more surface irregularities of pin specimen and disc are come in direct contact that means more metal to metal contact. That leads to more micro-weld formation between pin samples and disc. Now, when sliding occurs the material subjected to higher normal loading condition contributes to the more volume loss.

Generally, the wear test results are expressed as the specific wear rate. The specific wear rate is defined as the amount of volume loss per unit sliding distance [20]. Sometimes it may also expressed as amount of weight loss per unit sliding distance [11,18]. But, when applied load is also influencing parameter then specific wear rate can be defined as amount of volume loss per unit load per unit sliding distance. The slope of the above plot (Fig. 4.1) gives the value of cumulative volume loss to the sliding distance (mm^3/km) for each applied loading distance. From that result it can help to calculate specific wear rate of the material.

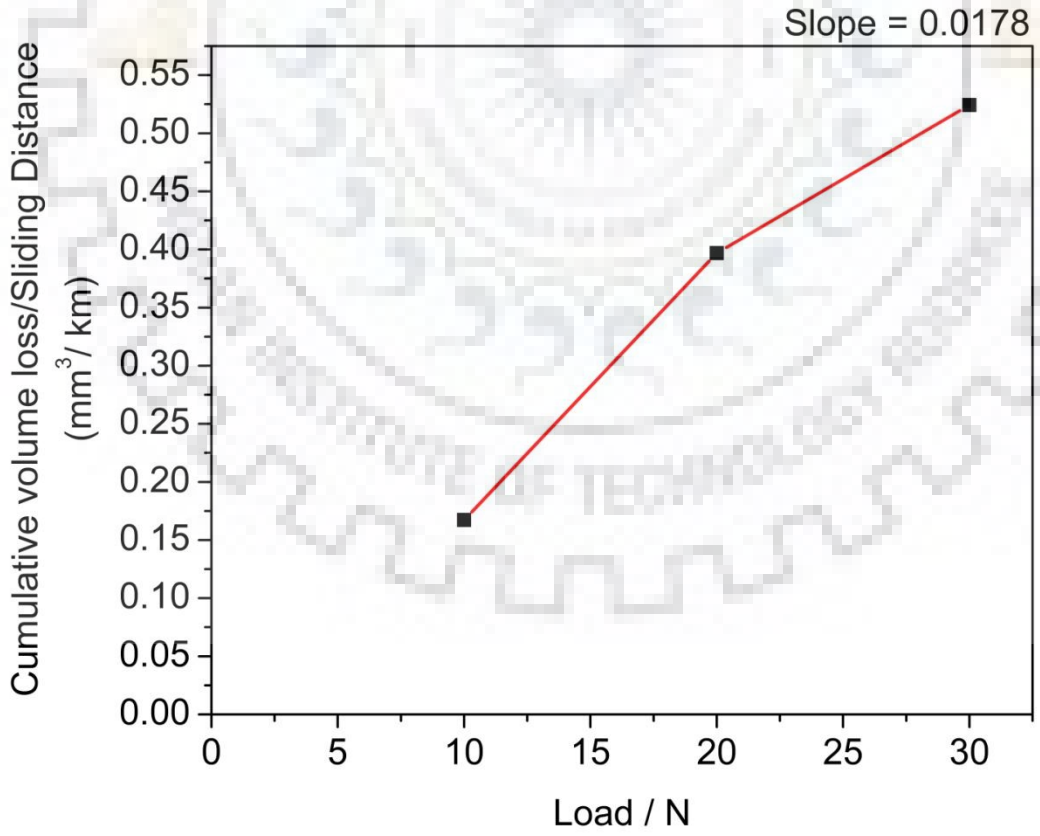

Figure 4.2: Plot of cumulative volume loss to the sliding distance as a function of load

The slope of the above graph (Fig. 4.2) is equal to 0.0178 $mm^3/km\,N$, and that is the specific wear rate of ultra high strength bainitic steel. This value of specific wear rate ($1.78 \times 10^{-5}\ mm^3/m\,N$) is compared with some other carbide free bainitic steel materials (Table 4.1) and that shows that the material is offering more wear resistance. Here, weight percentage of carbon is less compared to other alloy composition so the possibility of crack initiation due to hard phase particle i.e. carbides is limited. That can be the possible reason for showing good wear resistance of the chosen material.

Table 4.1: Comparison of specific wear rate for various composition of carbide free bainite

Alloy (wt%)	**Hardness**	**Specific wear rate** $(mm^3/m\,N)$	**Reference**
0.34C-1.51Si-1.80Mn-0.92Cr-0.015Al-0.032Ti	413 HV	1.78×10^{-5}	Present study
0.61C-1.72Si-0.75Mn-0.35Cr-0.12Ni	410 HV	1.0 to 1.6×10^{-4}	[32]
0.68C-1.60Si-1.25Mn-1.50Cr	589 HV	1.0×10^{-4}	[33]
0.98C-2.90Si-0.77Mn-0.45Cr	630 HV	0.9×10^{-4}	[33]

4.2 Surface topography

Surface roughness of pin samples were examined before and after wear as shown in the Fig. 4.3 using profilometer. The value of R_a at zero sliding distance is related to initial values of roughness of pin samples before wear. As expected, the average roughness (R_a) of the pin specimens increases, when samples are subjected to more sliding distance and to higher application of load. It is known facts that contact pressure become greater with rough surfaces compare to smooth surfaces, and it results into sub-surface plastic deformation of the material, which is extended up to some 15 to 20 microns, even though the nominal loading should leave the material in an elastic state.

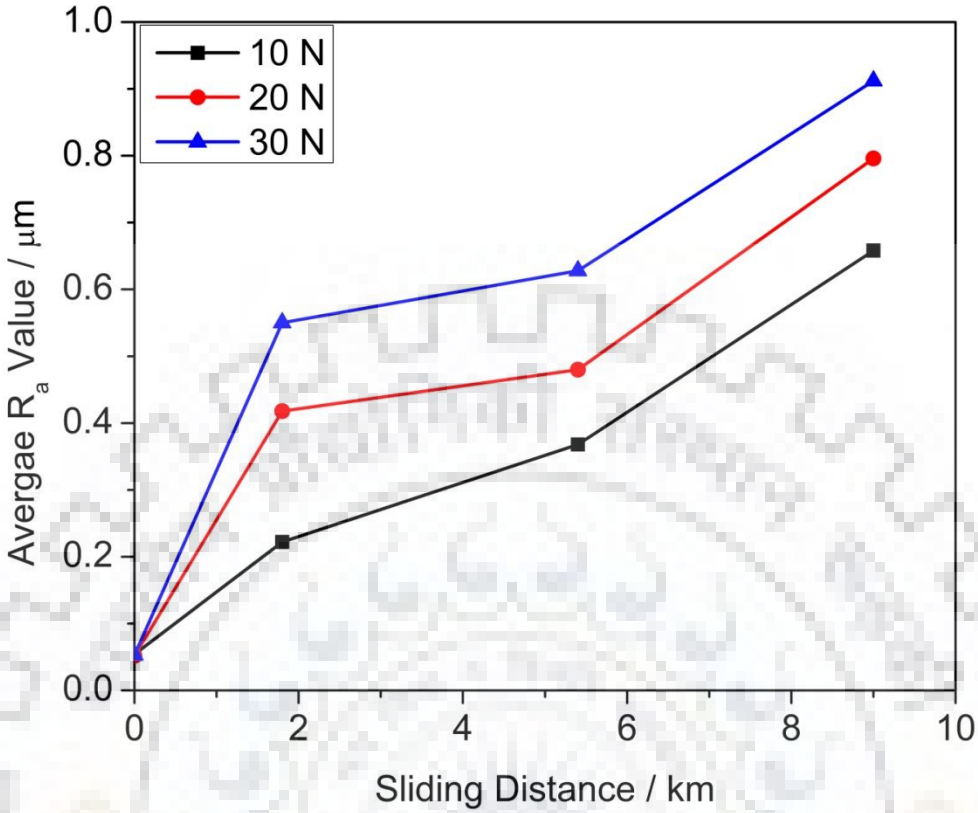

Figure 4.3: Plot of average roughness of pin samples to the sliding distance under 10,20 and 30 N loading condition

Atomic Force Microscopy (AFM) was used to know the 3D pattern of surface after wear. The line profile of the surface roughness in the direction perpendicular to wear tracks direction before and after wear under different loading condition is shown in the Fig. 4.4. The observation indicates that the distance between two consecutive crests and troughs are increases after wear. It becomes much wider for the samples subjected to higher loading condition. AFM results of pin samples also indicate that wear was uniform during the experiment and confirms that wear had happened on the complete circular surface of 6 mm diameter pins. Fig.4.5 shows 3D profile of wear tracks.

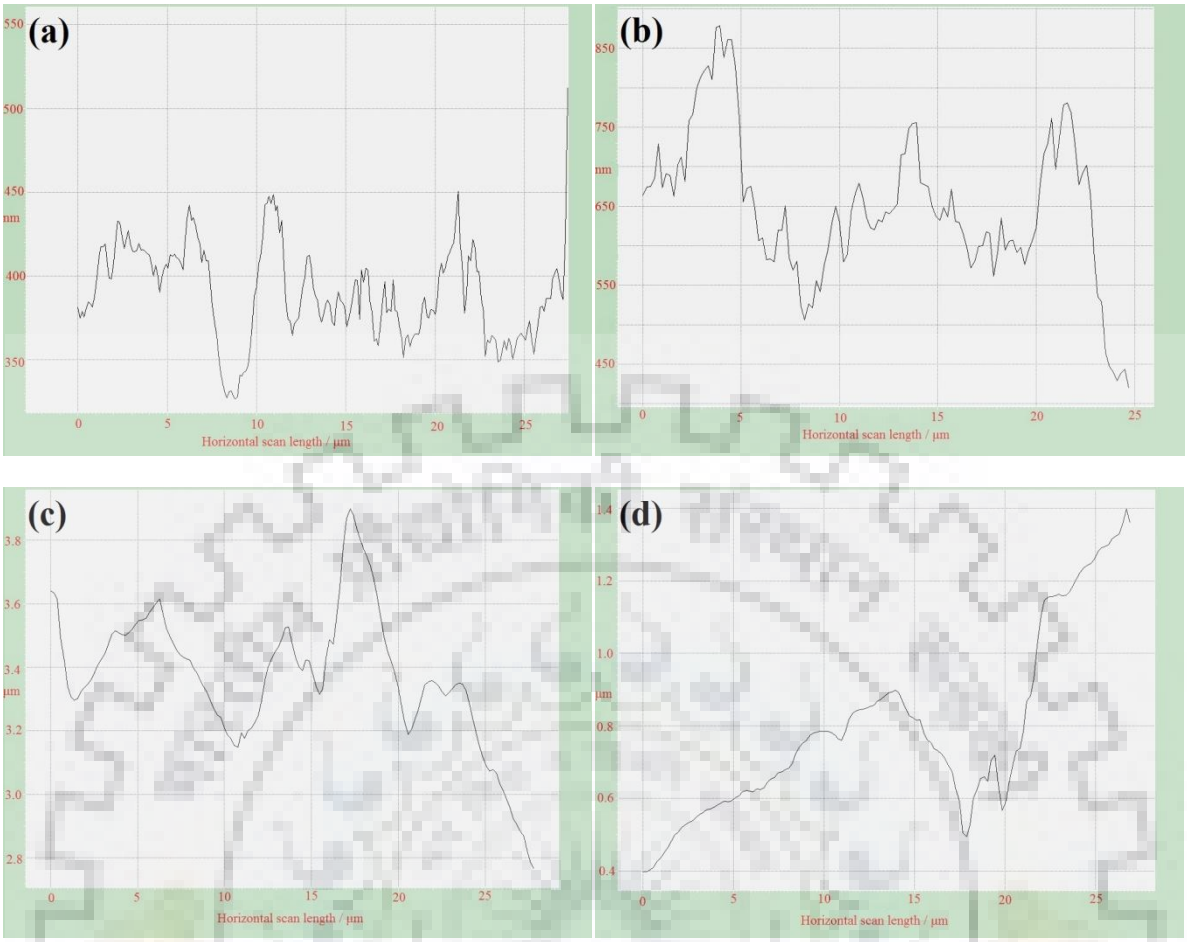

Figure 4.4: Line scan profile of the surface of the pin sample (a) before wear and after wear at (b) 10 N, (c) 20 N and (d) 30 N

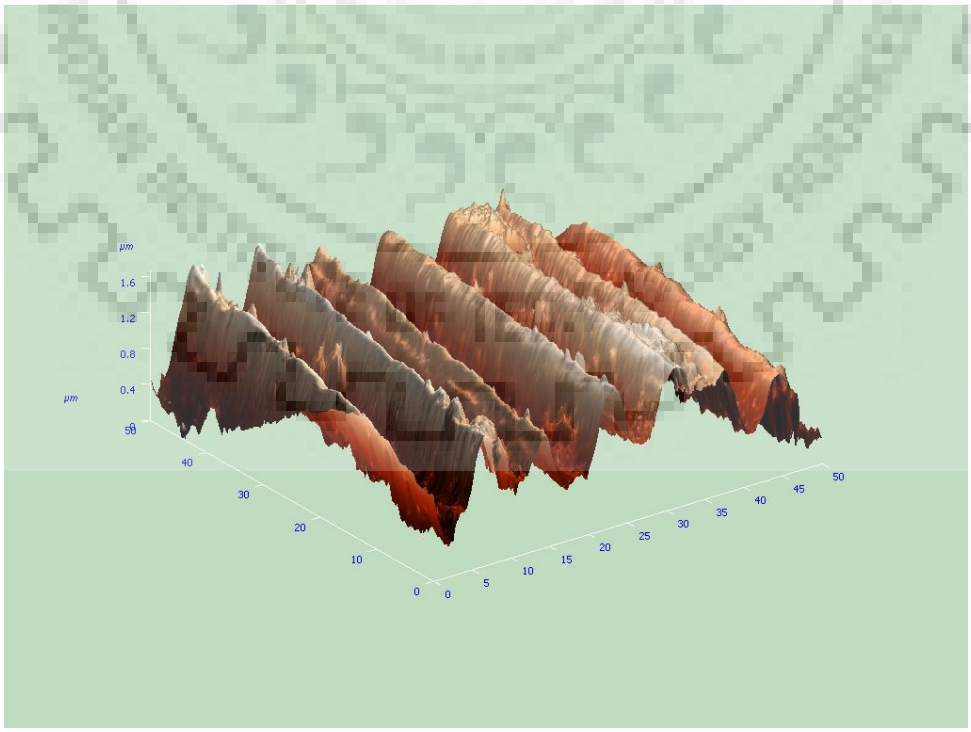

Figure 4.5: AFM images of bainitic pin samples after uniform wear at 20 N normal loading

4.3 Coefficient of friction

A coefficient of friction is the value that indicates the relationship between the force of friction between two surfaces and the normal reaction between the surfaces that are in contact. It was observed that when surface roughness of samples increases, coefficient of friction increases as well. Generally, the higher surface roughness indicates that real area contact of the surface is reduced, which generally (but not always) would mean a decrease in the friction coefficient. However it is also necessary to consider that orientation of roughness, because it may affect the coefficient of friction. When the specimens are in as machined or good polished conditions, the roughness as defined and uniform texture and that could be the reason that samples exhibit a low coefficient of friction in the run-in-stage. But, once texture obtained is worn off, the specimens start to show increase in the coefficient of friction until it reaches a steady state condition. It can be observed in the following Fig.4.6 for 20 and 30 N loading. But, results are contradictory for 10 N loading. It may be due to some unexpected errors in the instrument.

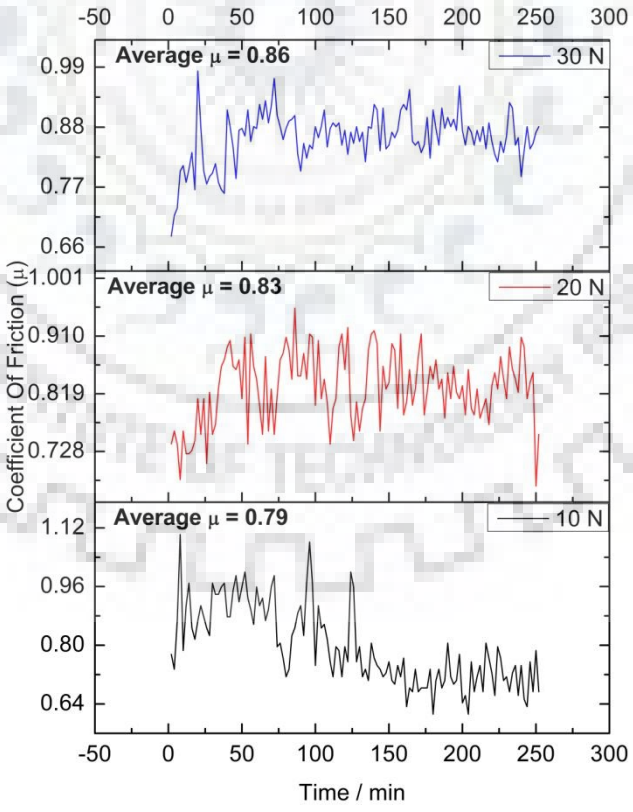

Figure 4.6: Coefficient of friction as a function of time for application of 10, 20 and 30 N loading condition

4.4 Microstructural characterization

4.4.1 Optical microscopy

The pin specimens were polished with 2000 grade silicon carbide emery paper before wear. To reveal the microstructure of as received samples Lepera (50 ml $Na_2S_2O_5$ 1% in aqueous dilution, 50 ml picric acid 4% in ethanol) etchant was used. Microstructure of as received ultra high strength bainitic steels shows mainly three phases. In the Fig.4.7 tiny bright region is untransformed (retained) austenite and the dark bluish colour is the region of bainite. Here, some darkest brown colour is the region of martensite phase.

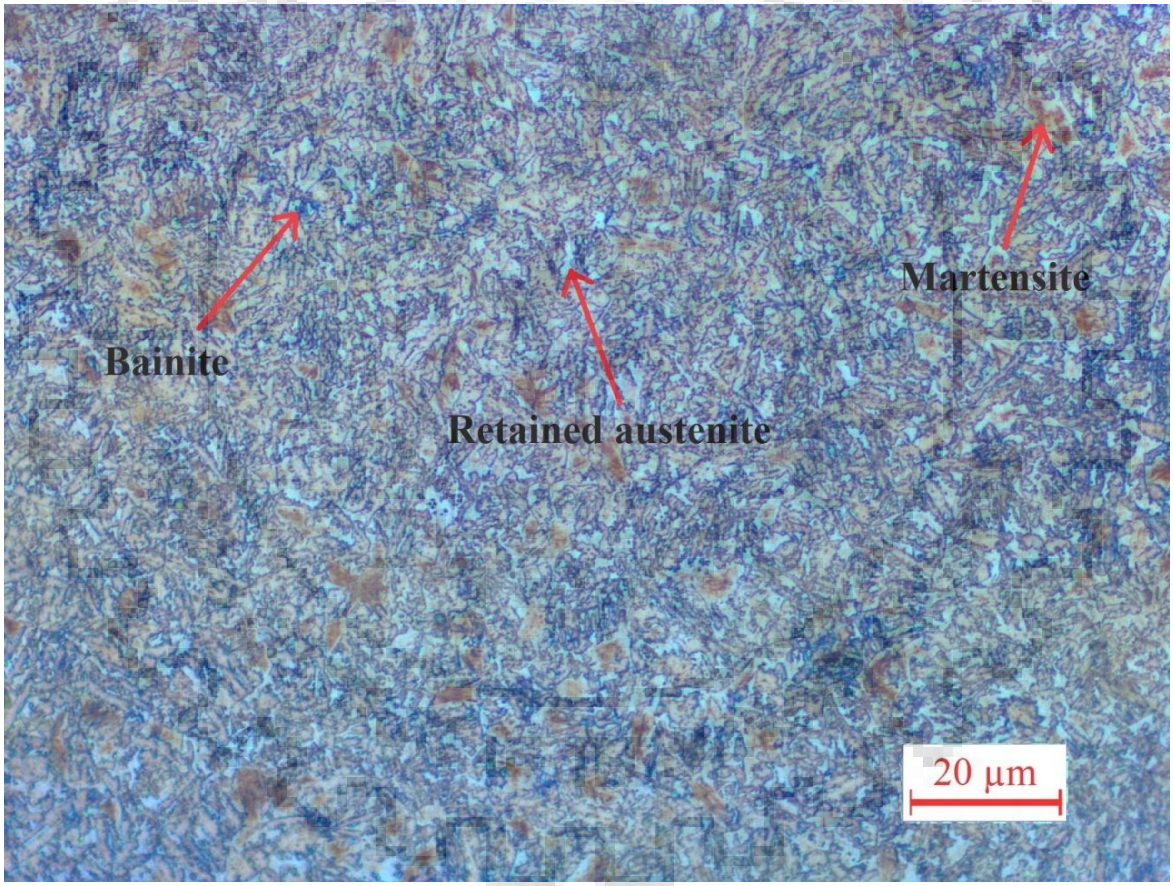

Figure 4.7: Optical micrograph of as received material at 500X magnification

During the sliding motions of pin samples the top surface is subjected to intense plastic deformation. The structure beneath the top surface experienced the strain hardening phenomena. To observe the effect of wear beneath the top surface, the cross-section of pin

samples were analysed using optical microscope. The observation shows that microstructure near the top surface has greatly refined. The presence of retained austenite has almost become negligible (Fig.4.8). It is expected that retained austenite has been transformed to martensite under extreme deformation experienced during wear. This should occur as the stability of retained austenite is not that great.

Figure 4.8: Optical micrographs of cross-section of the pin sample after wear

4.4.2 Scanning electron microscopy

Surface topography can completely reveal by scanning electron microscope. Fig.4.9 shows the typical surface of as received sample before the wear test. This SEM photograph of as received material is not showing the presence of any high temperature products like ferrite and precipitation of carbides in to or surroundings to the bainitic regions. Thus, the steel material confirms the microstructures having mainly two phases like retained austenite and bainitic ferrite. It is difficult to identify martensite phase by scanning electron microscope.

But, optical micrographs show the some fractions of martensite phase. Further, presence of austenite and ferrite phase can be identified by X-ray diffraction.

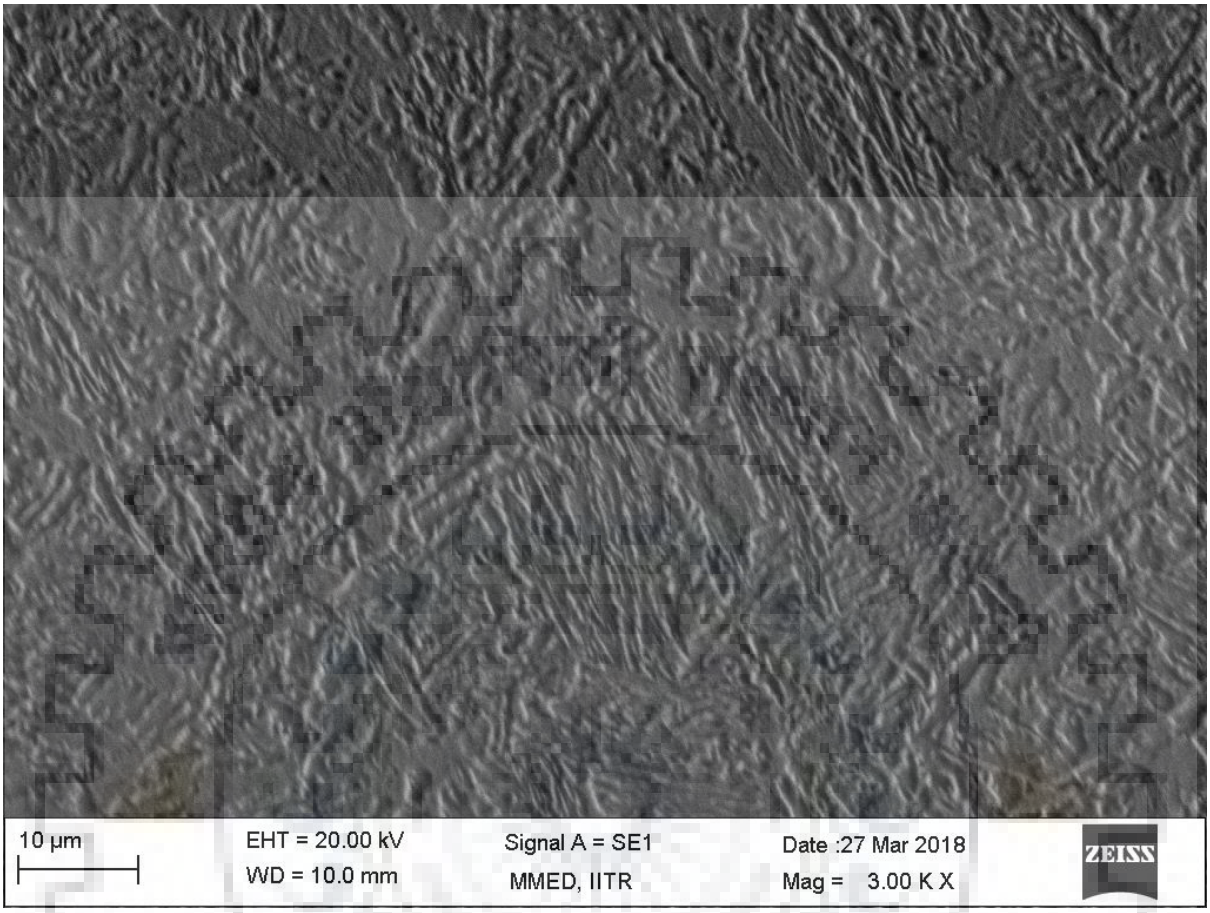

Figure 4.9: SEM image of as received sample before wear test

After the sliding wear test completed, all the worn samples were examined by SEM. Typical worn surface of pin samples at different loading condition are shown in the Fig. 4.10. From the Fig.4.10 it can be seen that intense formation of adhesion joints was observed in the pin samples, which is subjected to higher application of loading. And, pin sample subjected to lower loading shows very less pattern of wear tracks as shown in the Fig.4.10 (a). Wear tracks direction is easily visible under scanning electron micrographs. Wear has occurred in the complete circular area of pin samples and that is important point to consider for ideal case of wear testing.

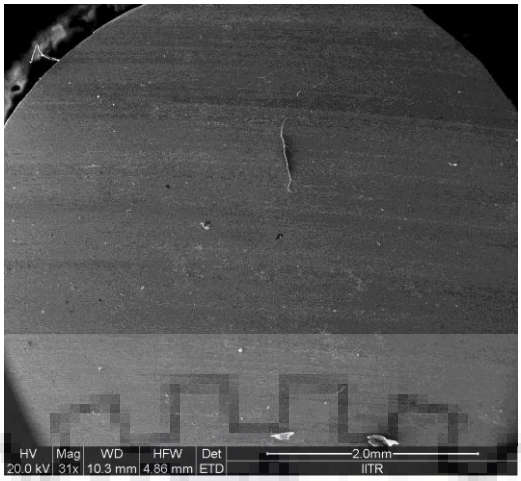

(a)

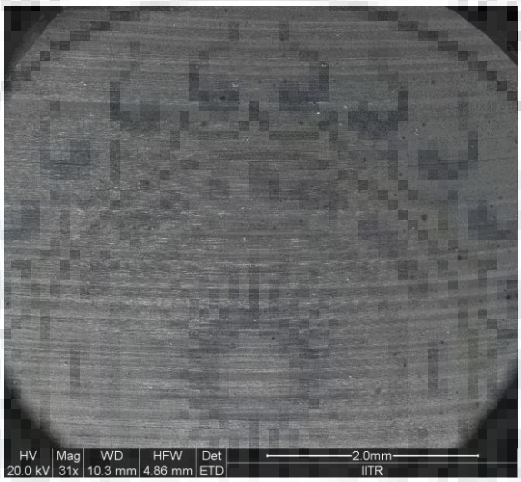

(b)

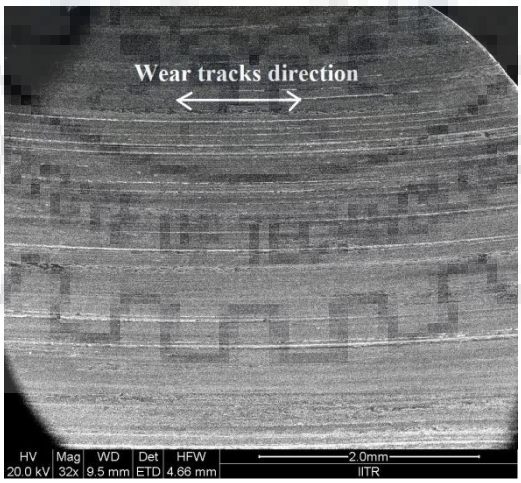

(c)

Figure 4.10: FE-SEM micrographs of worn surfaces of pin samples showing wear tracks directions for different load at (a) 10 N, (b) 20 N and (c) 30 N

The damage observed in different specimens, the material that has been removed from the pin samples is adhere on the top surface that can be easily seen in the Fig 4.11(a). The worn surface features can be closely examined in the Fig. 4.11. Typically, scar bed looks smooth. Wear debris, in the form of metallic flakes was not found to be attached on most of the pin samples. So, that there is confirmation of pure adhesive wear mechanism and absence of 'Type III' wear, which occurs due to mutual abrasion of wear debris generated. But, some amounts of oxides were observed in a few regions of some samples.

Possible explanations can be given for these different damages of material. The first explanation is that, there is a presence of retained austenite in the bainitic steels and due to that material is offering very high strength in combination of total elongation. Retained austenite is enriched in carbon content. Therefore, it is proposed that very fine and hard bright regions (retained austenite) protect the relatively softer ferrite matrix. And, this retained austenite phase worn out by asperity contact and shearing force and it lead to intra granular wear. That results into smoother wear scar bed in the samples (Fig. 4.10, 4.11(a)).

The second explanation is that, during the running in period elastic-plastic deformation of the surface asperities take place due to adhesion, and that results in the creation of crack nucleation sites in the surface as shown in the Fig.4.11(b). Another mechanism of damage is may be due to the small amount of wear debris that has oxidized and accumulated on the top surfaces are hard enough to cause indentation damage. It may be possible that wear debris gets pile up at the contact opening and then pressed inside the contact. This can also lead to plastic deformation of the surfaces. Fig.4.12 shows the EDX spectra of the sample where high presence of oxygen, iron, chromium, silicon, cobalt, manganese, etc. This results shows that wear debris produce is oxidized during the test because of localized heating due to friction.

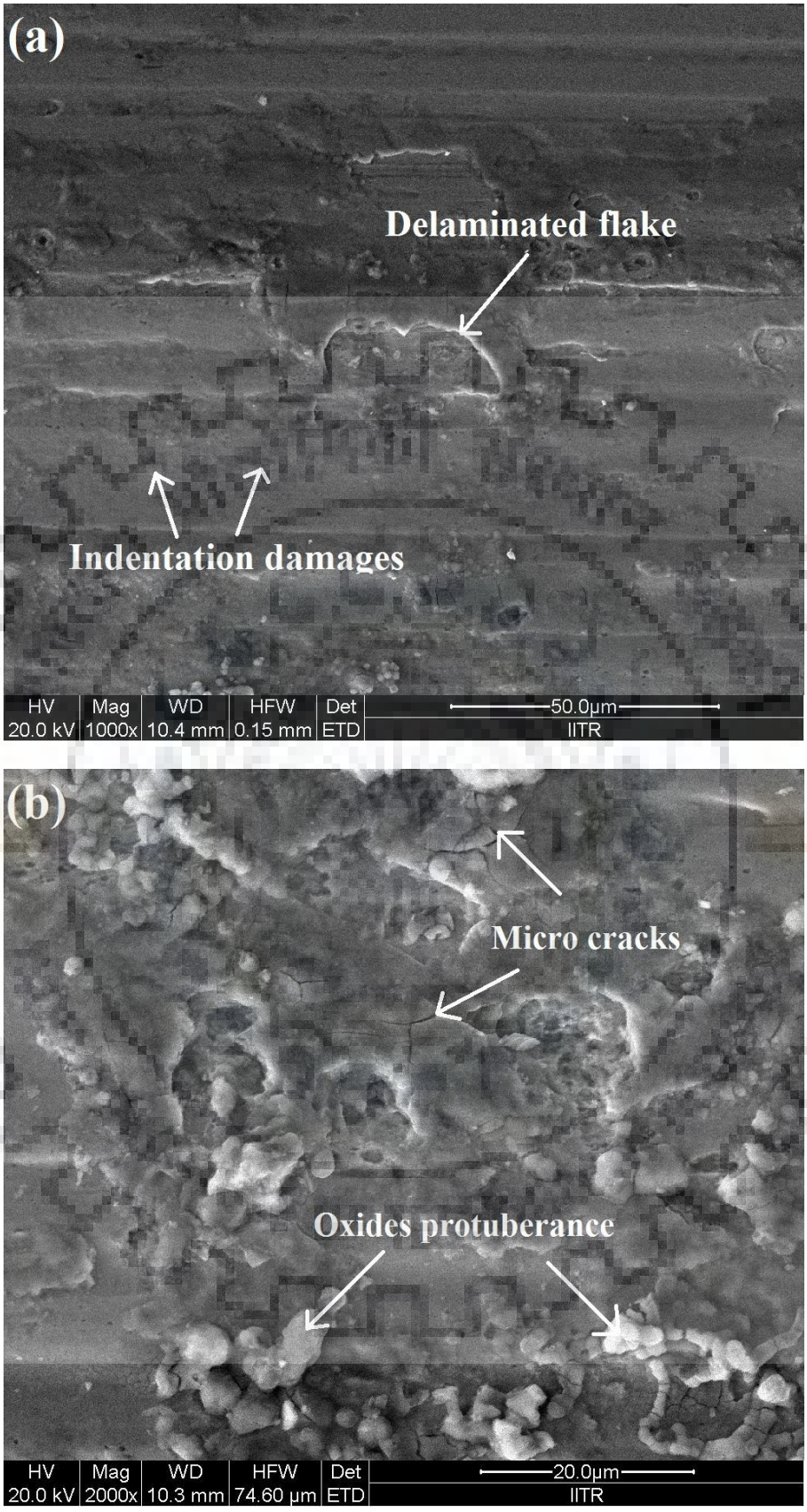

Figure 4.11: FE-SEM micrographs of pin samples after wear test (a) showing delaminated flakes, indentation damages, wear tracks (b) showing micro cracks, oxides protuberance

(a)

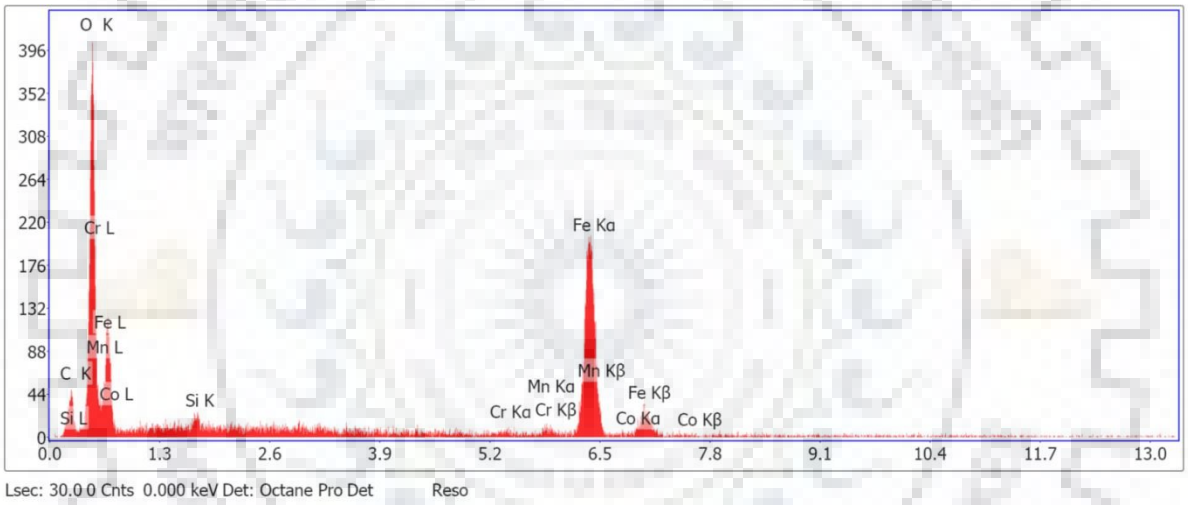

(b)

Figure 4.12: (a) FE-SEM micrographs of oxidized wear debris accumulated on the top of deformed surface of pin sample and (b) EDS spectra of pin specimen tested at 10 N loading

It is also interesting to observe the cross-section of the worn surface (Fig. 4.13), there is a little damages to the nanostructure bainite like sub-surface cracks as observed in the case of other bainitic steels[32,33]. The region of top surface has suffered heavy plastic deformation. The material damage was observed within less than 15 μm depth from the top surface even for higher loading. The microstructure of region beneath this highly deformed region is different from the bulk region of sample. The same samples were examined in the optical microscope and some lath shaped martensite was observed (Fig.4.8). At higher

loading, it was observed that plastic deformation become so intense that material gets damaged and many surface and sub-surface cracks are generated as shown in the Fig.4.13(c).

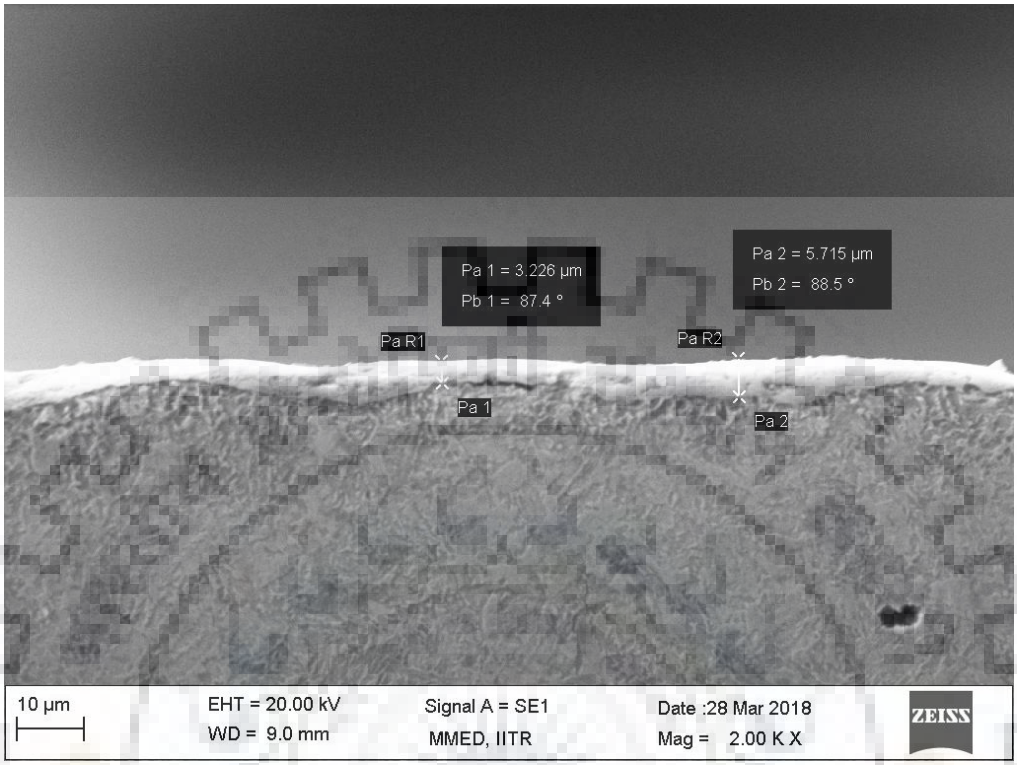

(a)

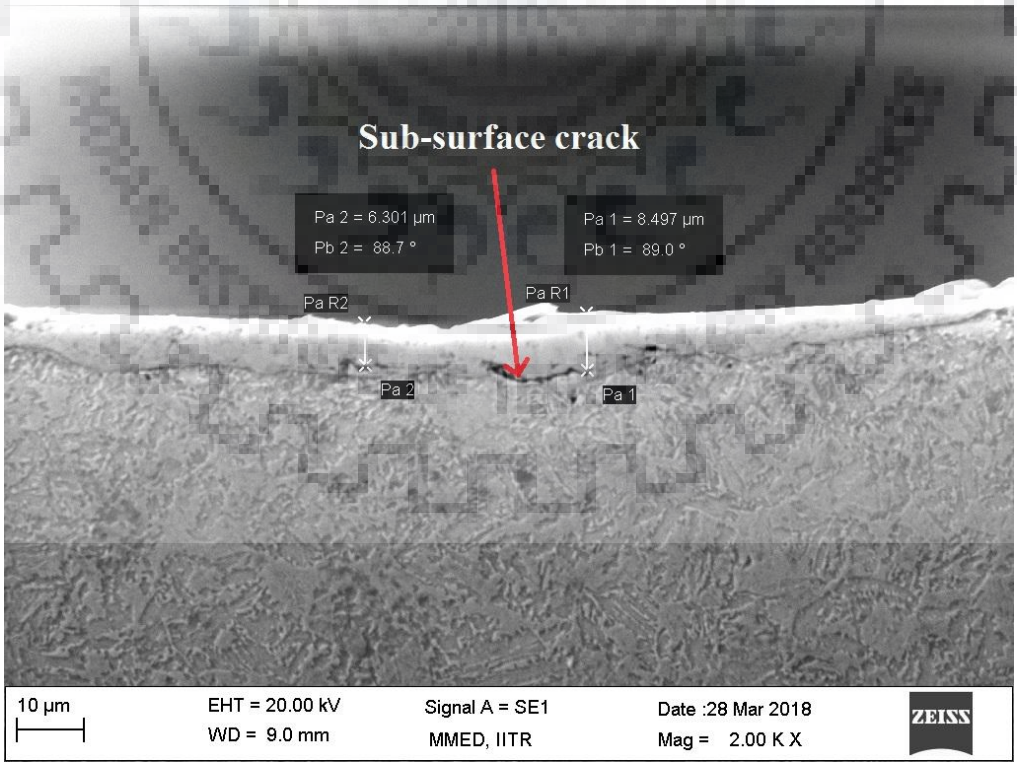

(b)

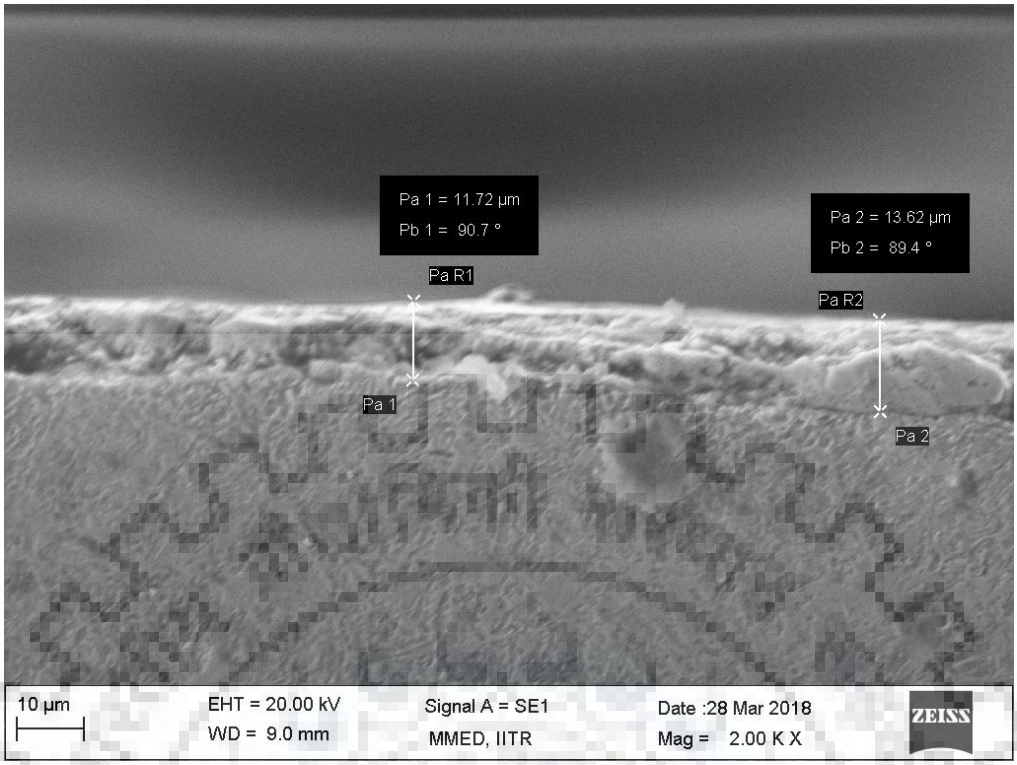

(c)

Figure 4.13: The cross-section of pin samples showing highly deformed region and sub-surface cracks under different loading condition (a) 10 N (b) 20 N and (c) 30 N

4.4.3 Nanoindentation results

Nanohardness was measured on the polished cross-section surface. To understand the distribution of hardness in the strain harden region the data were collected from the depth of top surface, which was under the sliding motion. As hardness of material before wear was nearly 413 Vicker hardness number and it is equal to 4.05 GPa. The results indicate that layer in the vicinity of the top surface subjected to more strain hardening and showing higher values of hardness. And, the surface which is a far away from the top surface showing decreases in the hardness (Fig.4.14). In this case, depth of deformation zone is larger as compared to previous research[30]. One possible reason is the strain induced transformation of austenite phase to hard martensite phase. Possibly, this would make material more wear resistance. Normal loading is also affecting the hardness of the material. At higher loading, more material is subjected to plastic deformation and that leads to increase in dislocation density and ultimately it shows the higher value of hardness (Fig.4.15). Presence of martensite phase is also observed in the Optical microscope (Fig.4.8).

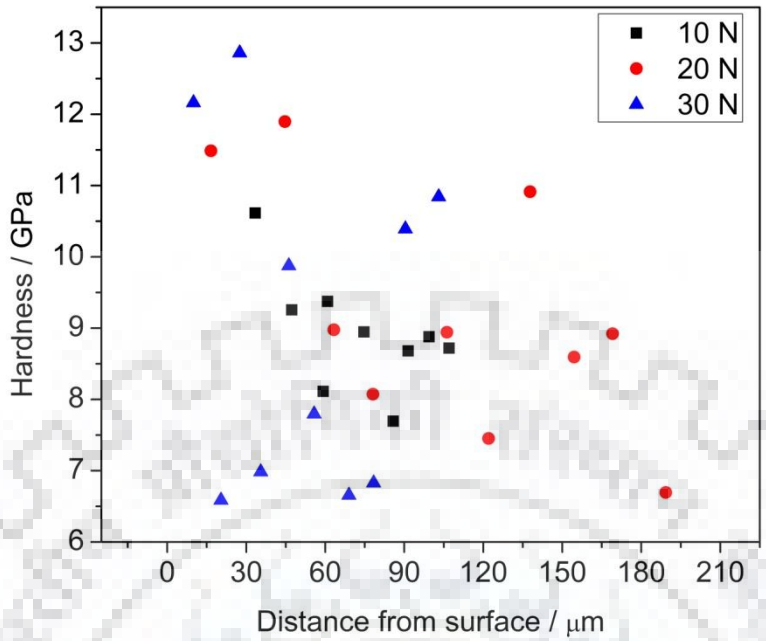

Figure 4.14: Distribution of nanohardness of the subsurface layers after wear

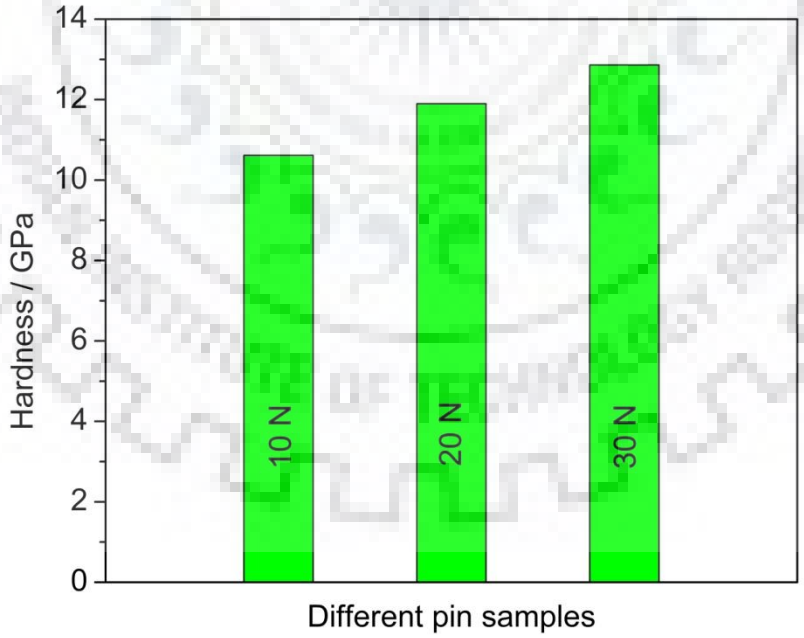

Figure 4.15: Maximum magnitude of hardness under different loading condition

4.4.4 X-ray diffraction

X-ray diffraction pattern of material in as received condition is illustrated in the Fig. 4.15. The quantitative phase analysis using full pattern Rietveld analysis was done using MAUD software. Individual reflections from the diffracting planes of fcc-austenite (γ) and bcc-ferrite (α) are labelled in the Fig. 4.16. Bragg reflections from the α (110), α (200), α (211), α (220) planes along with γ (111), γ (200), γ (220), γ (311), γ (222) reflections could be identified over the scanned 2θ range. Peaks of bcc-ferrite and bct-martensite had less than 0.1º seperations and therefore could not be identified. But optical microscope of material confirms the presence of martensite (Fig. 4.7).

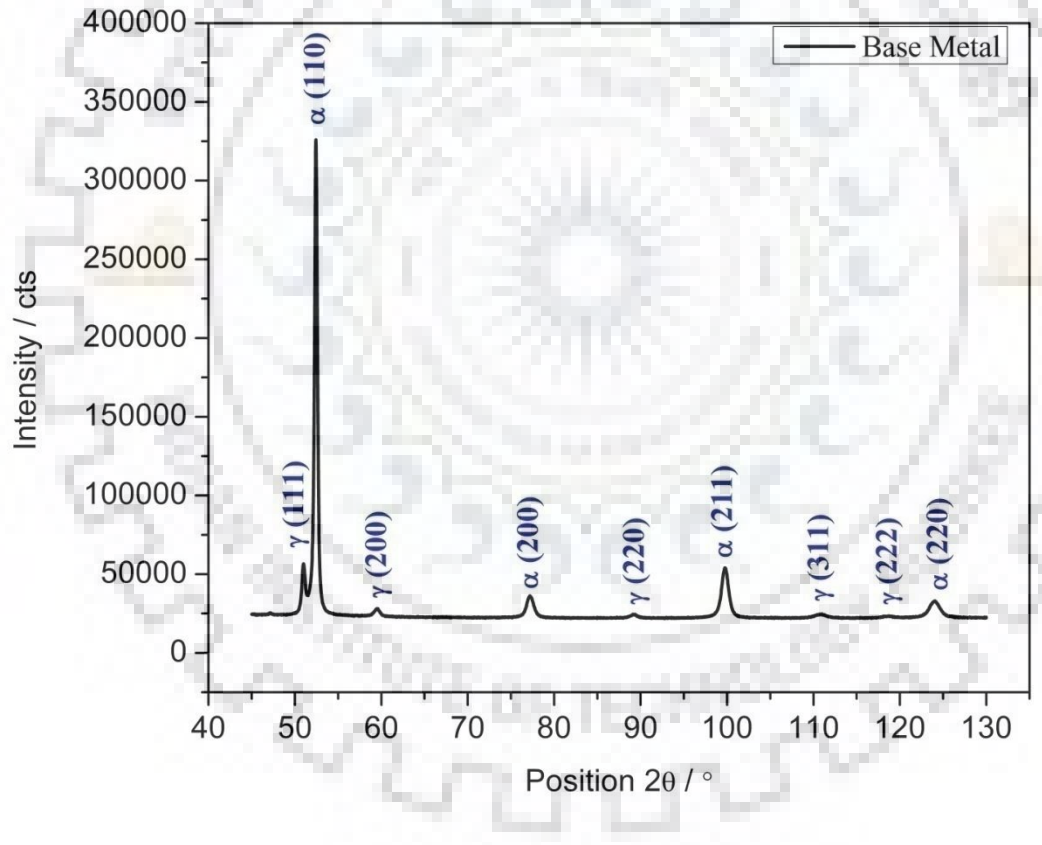

Figure 4.16: X-ray diffraction pattern of ultra high strength bainitic steel before wear testing

.

X-ray diffraction pattern of pin specimen was examined after wear testing. As the temperature during experiments did not go beyond 29º C, the possibility of re-austenitisation of ferrite and subsequent transformation to martensite is neglected. But, the relative intensity

of the austenite peaks was diminished after wear testing as shown in the Fig. 4.17. That indicates the strain-induced transformation of austenite into martensite. It is interesting to note that intensity of austenite peaks decreases gradually as the application of load increases from 10 to 30 N (Fig.4.17). The x-ray diffraction pattern for all the samples were analysed using MAUD software. The quantitative phase fractions were determined using standard crystallographic information file (CIF) of ferrite and austenite. It was difficult to find phase fraction of martensite because it has less than 0.1ºC separations form ferrite peaks and software was also not capable of determined the phase fraction of three phases simultaneously. The direct conclusion can be made that phase fraction of martensite after wear testing is nearly equal to the difference of phase fraction of retained austenite before and after wear testing. Phase fraction of retained austenite after wear is shown in the Fig. 4.18.

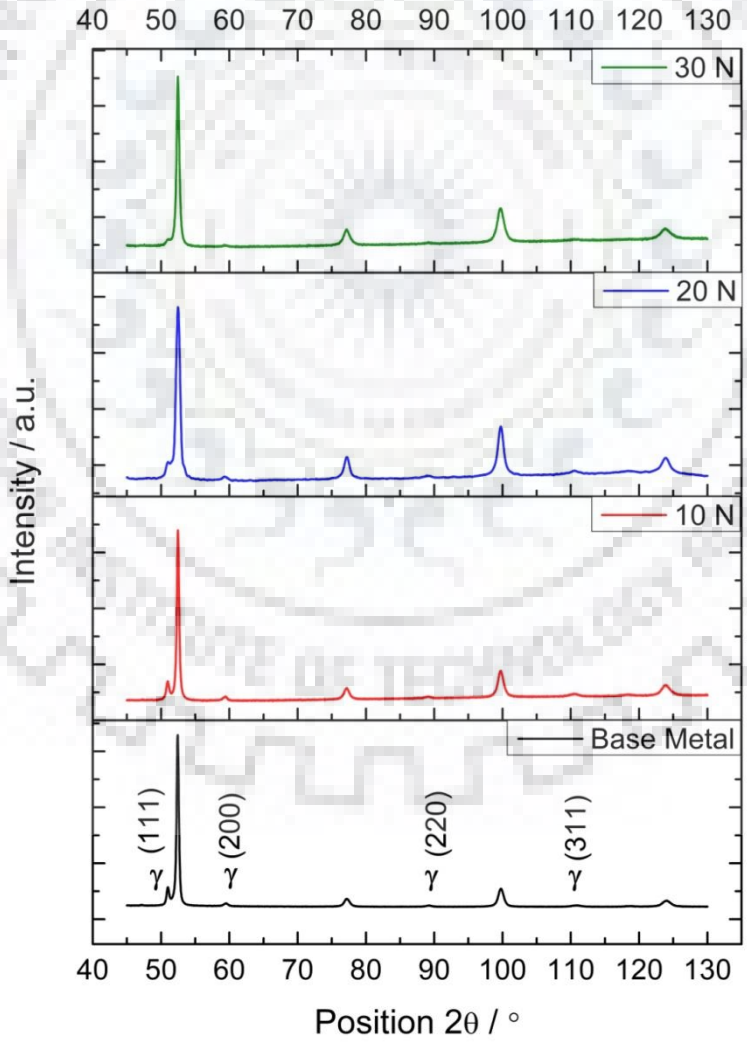

Figure 4.17: X-ray diffraction pattern of bainitic pin samples before and after wear showing strain induced transformation of retained austenite at 10 N, 20 N, and 30 N loading

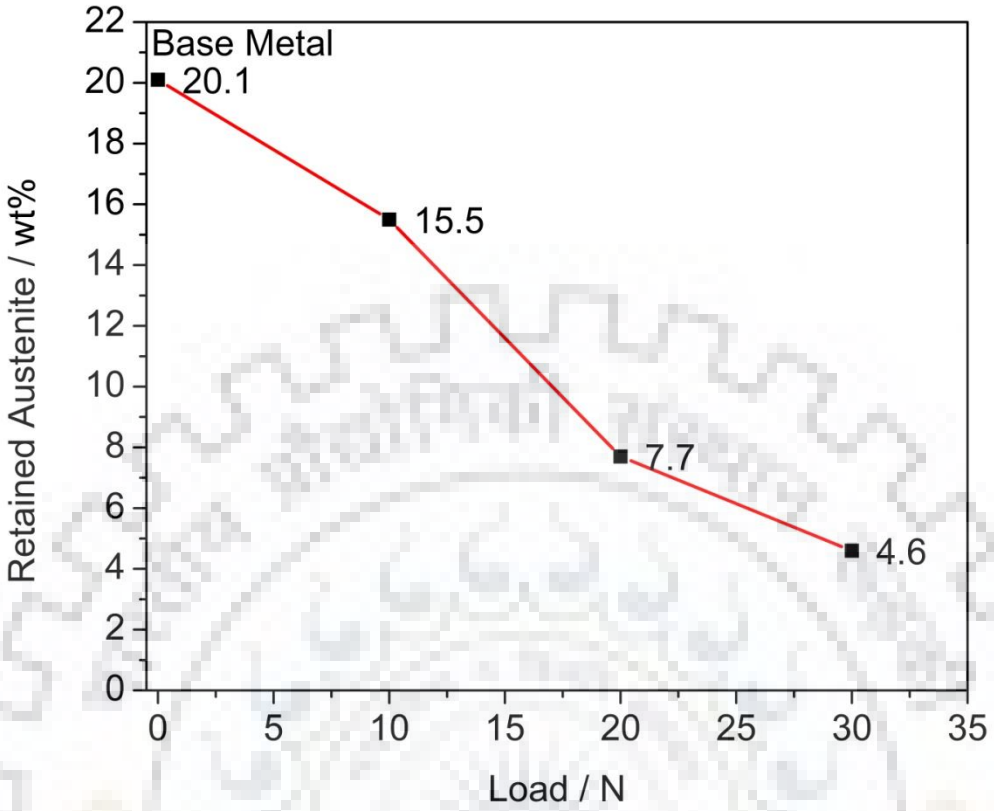

Figure 4.18: Variation in weight percentage of retained austenite phase under different loading condition

It is interesting to note that weight percentage of austenite is decreasing with increment of load. The austenite is present in a finely divided state and a reduction in the grain size of austenite reduces its martensite start temperature [34,35]. In this case, thermal activation does not play role in the growth of martensite phase. However, the deformation that the material has experienced is capable of causing deformation induced transformation of γ to its product phase α'. In this way, the material also gets strain hardened. Dislocations might be playing an important role in martensitic transformations. Dislocations in the austenite phase clearly provide sites for heterogeneous nucleation. So, the formation of microscopic slip leads to macroscopic deformation. Furthermore, the transformation of γ to α' leads to volume expansion, it can result into an increase in dislocation density. This increase in dislocation density can affect the XRD profile as well.

The broadening of X-ray diffraction peaks was studied further to examine the structural changes due to wear, associated with the retained austenite, crystallite size, strain, dislocation density, etc. The Williamson-Hall plots for austenite of pin samples before and after wear are shown in the Fig.4.19. The linear curve fitting equation is also shown in the Fig. 4.19. The slope of the equation is equal to 4ε, and that gives the value of strain (ε) in the material. The intercept is equal to $k\lambda/D$ and that determines the crystallite size (D). After wear, data points in the Williamson-Hall plot are not in a straight line. One possible reason is that, there is anisotropic strain distribution in some preferred crystallographic planes than others. So, there is a non-monotonic change in FWHM of X-ray diffraction.

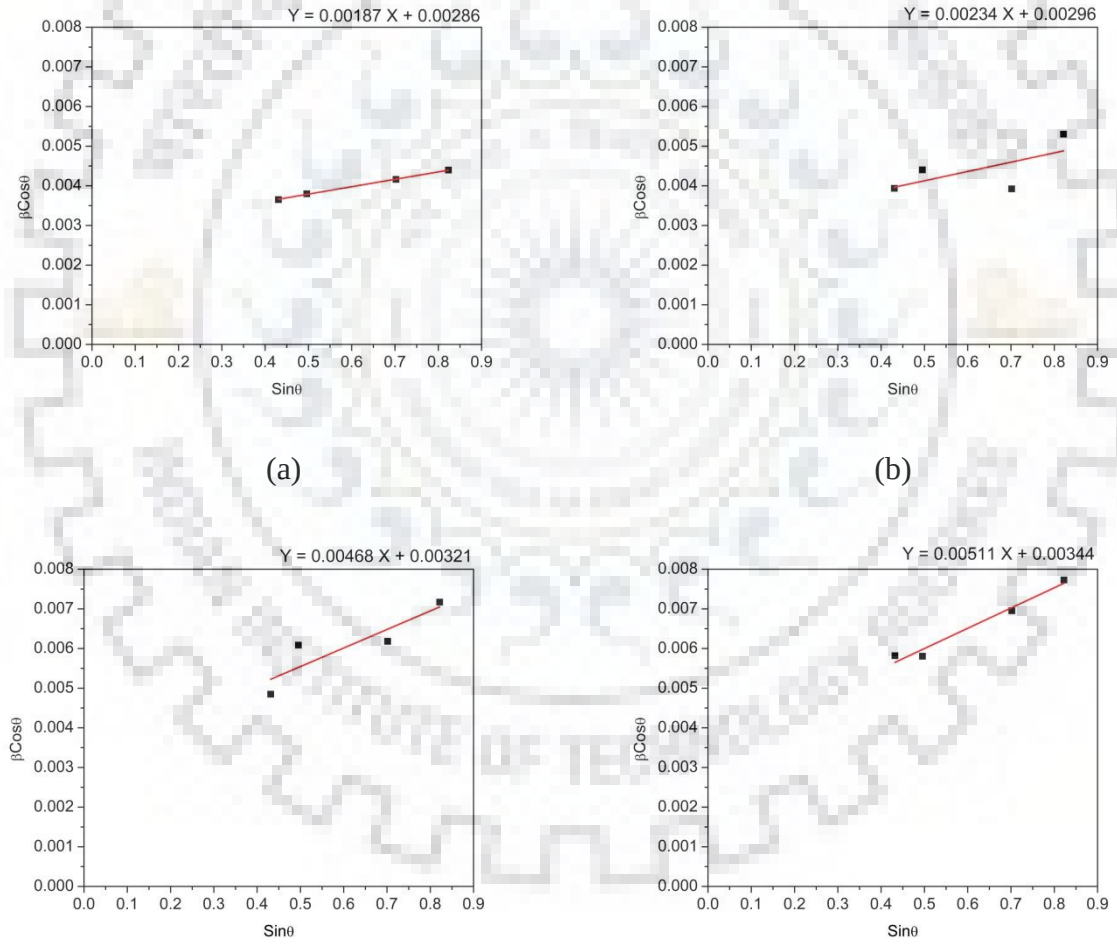

Figure 4.19: Williamson-Hall plot for austenite (a) before wear (b) after wear at 10 N load (C) after wear at 20 N load and (d) after wear at 30 N load

Crystallite size, strain and dislocation density were calculated from the Williamson-Hall plot. Here, showing complete procedure for material used before wear testing (Fig. 4.19(a)).

Calculations:

y = 0.00187 x + 0.00286

Strain and crystallite size of austenite,

Slope of the graph = $4\epsilon = 0.00187$

So, Strain = $\epsilon = 0.0004675$

Intercept = $\frac{K\lambda}{D} = 0.00286$; where K = 0.9 , $\lambda = 1.789$ A^o,

So, D = 562.97 A^o

Dislocation density of austenite,

$$\rho = \frac{\sqrt{12}\ \varepsilon}{bd},$$

b = burger's vector = $\frac{a}{2}\sqrt{h^2 + k^2 + l^2}$

b for Austenite = $\frac{3.1005123}{2}\sqrt{1^2 + 1^2 + 1^2} = 2.68512$ A^o

Dislocation density $\rho = \frac{\sqrt{12}\ 0.0004675}{2.68512 * 2.0772} \times 10^{14} = 0.00029036 \times 10^{14} = 2.9036 * 10^{10}$ mm^{-2}

It is important to understand the relation between dislocation motion and mechanical behaviour of metal. At macroscopic level, plastic deformation of material is corresponds to large number of dislocations movement. The dislocation density in a material increases with the amount of plastic deformation, due to dislocation multiplication or the formation of new dislocations. In this case, Normal load (10 to 30 N) is corresponds to the amount of plastic deformation or cold work. So, dislocation density increases with application of normal load on the specimens (Fig. 4.20). Now, due to increase of dislocation density, the average distance between dislocations decreases. That means dislocations are positioned closed together. On an average, dislocation-dislocation strain interactions are repulsive. Due to that

motion of dislocation is hindered by presence of adjacent dislocations. As the dislocation density increases, the resistance to dislocation motion by other dislocations becomes more active. That results into strain-hardening of the material. The plot of strain against different loading condition is shown the Fig. 4.21. The variations in crystallite size before and after wear under different condition of loading are shown in the Fig. 4.22. As expected, the crystallite size decreases with increment of applied load. The size of the austenite region has been greatly refined, by the formation of martensite.

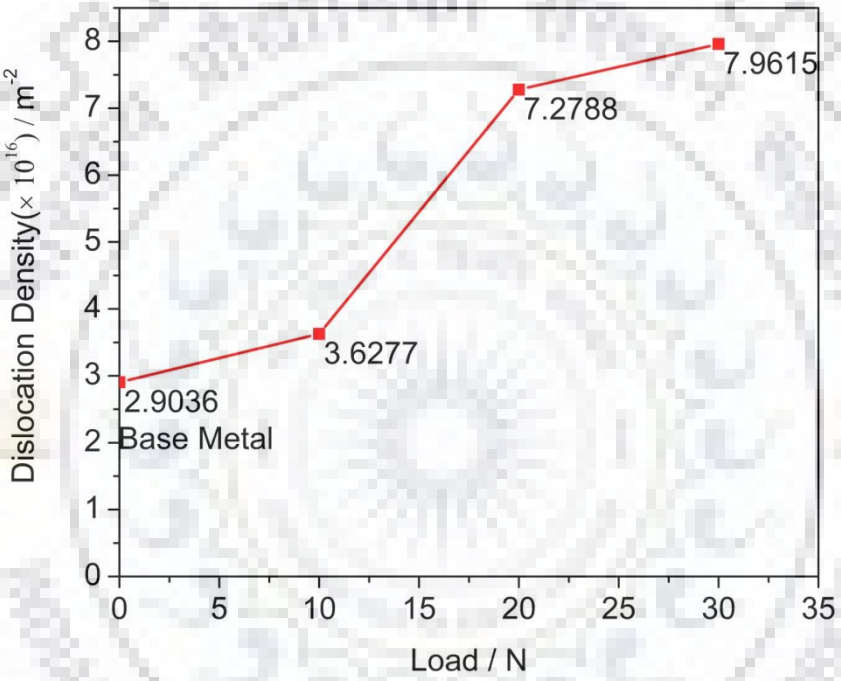

Figure 4.20: The plot of dislocation density against loading parameter

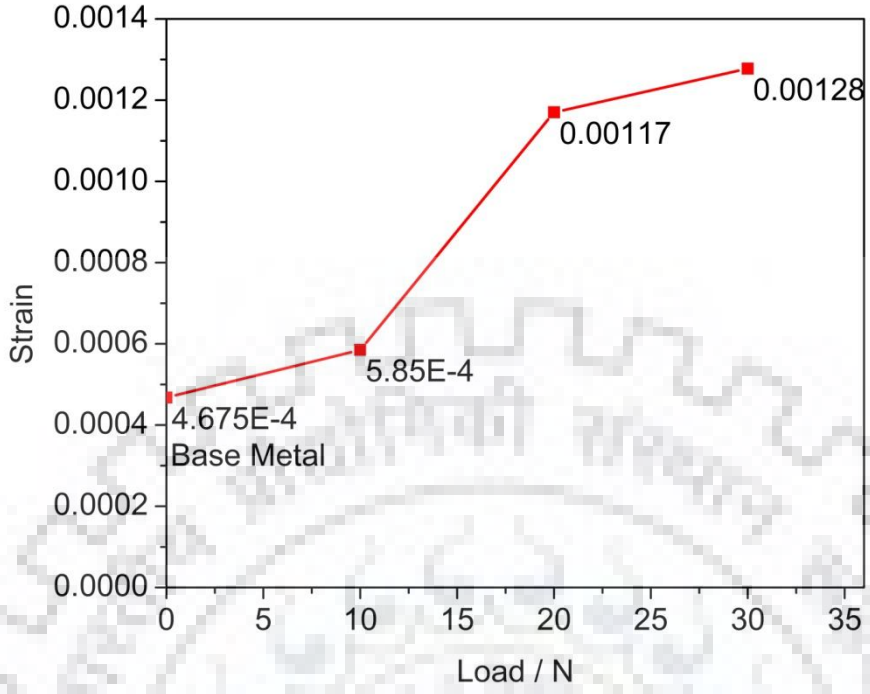

Figure 4.21: The plot of strain induced in the material under different loading condition

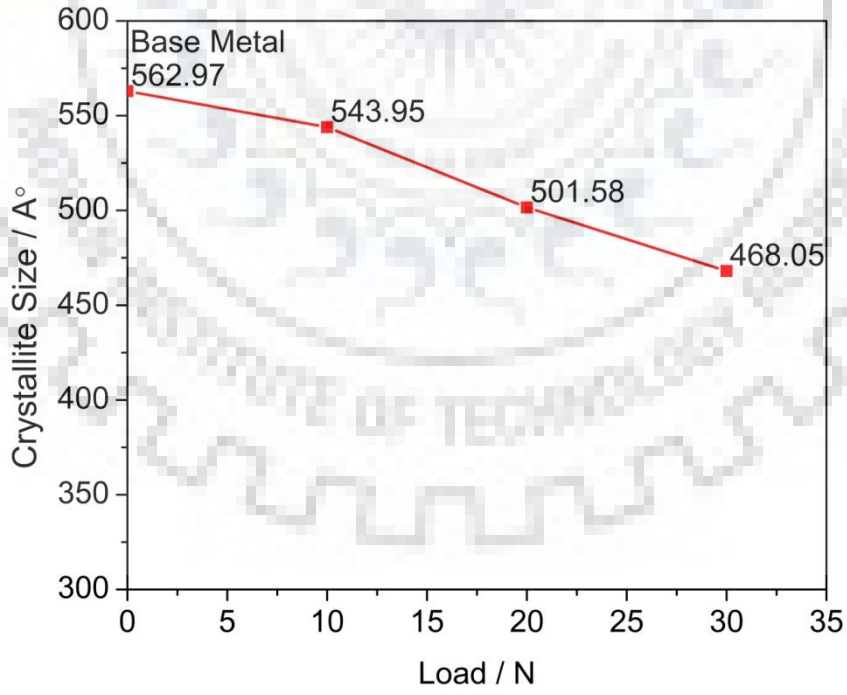

Figure 4.22: The variations of crystallite size before and after wear under different loading condition

Chapter 5

CONCLUSIONS AND FUTURE SCOPE

5.1 Conclusions

The adhesive wear behaviour of ultra high strength and carbide-free bainitic steel has been examined and following general conclusions can be drawn from the combinations of experimental works and theoretical analysis:

- The specific wear rate of material is $1.78 \times 10^{-5}\ mm^3/m\ N$, which is lower than other nano-structured carbide-free bainitic steel studied previously, even though the hardness is less than that observed in the previous work.
- The retained austenite content is about 20% in as received material and this provides the mechanism of strain-hardening that leads to an increase in hardness of the material after wear test.
- Nanohardness of the material has increase significantly and possibly it is due to strain induced transformation of retained austenite phase into hard martensite phase.
- The results of scanning electron microscopy indicate that the material damage was observed within less than 15 μm even for higher loading application.
- X-ray diffraction analysis and optical micrographs indicate that retained austenite is directly transform to hard phase martensite and that further helps to improve wear resistance of the material.

5.2 Future scope

- Performance of the material is directly affected by the environmental condition and its application. In this study focus was made to analyse the performance of the material by considering the pure adhesive wear phenomena. Material performance was good under this condition. So, it can be used as the rail tracks material.

- But, it is also necessary to check material performance for different mechanism of wear. The same material can be tested for erosive wear, abrasive wear, etc. to ensure its best suitable application.
- The material can be heat treated to change its microstructure (martensite) and some mechanical properties (like hardness). Performance of this heat treated material can also be tested by above mention mechanism of wear.
- It would be interesting to do detail characterization of worn surfaces to understand the exact damage mechanism in all the types of wear.

REFERENCES

[1] Hutchings I, Shipway P. Tribology: friction and wear of engineering materials. Butterworth-Heinemann; 2017 Apr 13.

[2] Das S, Haldar A. Continuously cooled ultrafine bainitic steel with excellent strength–elongation combination. Metallurgical and Materials Transactions A. 2014 Apr 1;45(4):1844-54.

[3] Bosnjak B, Asanovic V, Radulovic B, Pop-Tonev K. Influence of microalloying and heat treatment on the kinetics of bainitic reaction in austempered ductile iron. Journal of Materials Engineering and Performance. 2001 Apr 1;10(2):203-11.

[4] Eyre TS, The mechanisms of wear. Tribology International Volume 11, Issue 2, Apr 1978, 91-96.

[5] Rabinowicz E. Tribology ii, video course mannual. Center for Advanced Engineering Study, Cambridge, MA. 1983:1-2.

[6] Kalousek J, Fegredo DM, Laufer EE. The wear resistance and worn metallography of pearlite, bainite and tempered martensite rail steel microstructures of high hardness. Wear. 1985 Oct 1;105(3):199-222.

[7] Garnham JE, Beynon JH. Dry rolling-sliding wear of bainitic and pearlitic steels. Wear. 1992 Aug 14;157(1):81-109.

[8] Clayton P, Devanathan R, Jin N, Steele RK. A review of bainitic steels for wheel/rail contact. InRail Quality and Maintenance for Modern Railway Operation 1993 (pp. 41-51). Springer, Dordrecht.

[9] Danks D, Clayton P. Comparison of the wear process for eutectoid rail steels: field and laboratory tests. Wear. 1987 Dec 1;120(2):233-50.

[10] Clayton P, Danks D. Effect of interlamellar spacing on the wear resistance of eutectoid steels under rolling-sliding conditions. Wear. 1990 Jan 1;135(2):369-89.

[11] Jin N, Clayton P. Effect of microstructure on rolling/sliding wear of low carbon bainitic steels. Wear. 1997 Jan 1;202(2):202-7.

[12] Viafara CC, Castro MI, Velez JM, Toro A. Unlubricated sliding wear of pearlitic and bainitic steels. Wear. 2005 Jul 1;259(1-6):405-11.

[13] Clayton P. The relations between wear behaviour and basic material properties for pearlitic steels. Wear. 1980 Apr 1;60(1):75-93.

[14] Bolton PJ, Clayton P. Rolling—sliding wear damage in rail and tyre steels. Wear. 1984 Jan 16;93(2):145-65.

[15] Clayton P, Sawley KJ, Bolton PJ, Pell GM. Wear behavior of bainitic steels. Wear. 1987 Dec 1;120(2):199-220.

[16] Devanathan R, Clayton P. Rolling-sliding wear behavior of three bainitic steels. Wear. 1991 Dec 20;151(2):255-67.

[17] Clayton P, Devanathan R. Rolling/sliding wear behavior of a chromium-molybdenum rail steel in pearlitic and bainitic conditions. Wear. 1992 Jul 15;156(1):121-31.

[18] Clayton P, Jin N. Unlubricated sliding and rolling/sliding wear behavior of continuously cooled, low/medium carbon bainitic steels. Wear. 1996 Dec 1;200(1-2):74-82.

[19] Jin N, Clayton P. Effect of microstructure on rolling/sliding wear of low carbon bainitic steels. Wear. 1997 Jan 1;202(2):202-7.

[20] Shipway PH, Wood SJ, Dent AH. The hardness and sliding wear behaviour of a bainitic steel. Wear. 1997 Mar 1;203:196-205.

[21] Heller W, Schweitzer R. Hardness, microstructure and wear behavior of steel rails. InProc. 2nd Int. Heavy Haul Railway Conf. 1982 Sep 25 (pp. 282-286). AAR Chicago.

[22] Ichinose H, Takehara J, Ueda M. High strength rails produced by two stage flame heating and slack quenching. In2nd International Conference on Heavy Haul Railways, Colorado Springs, USA 1982 Sep (pp. 178-182).

[23] Kalousek J, Fegredo DM, Laufer EE. The wear resistance and worn metallography of pearlite, bainite and tempered martensite rail steel microstructures of high hardness. Wear. 1985 Oct 1;105(3):199-222.

[24] Chattopadhyay C, Sangal S, Mondal K, Garg A. Improved wear resistance of medium carbon microalloyed bainitic steels. Wear. 2012 Jun 15;289:168-79.

[25] Vuorinen E, Wang L, Stanojevic S, Prakash B. Influence of retained austenite on rolling-sliding wear resistance of austempered silicon alloyed steel. InInternational Conference on Hot Sheet Metal Forming of High-Performance Steel: 15/06/2009-17/06/2009 2009 (pp. 339-347). Verlag Wissenschaftliche Scripten.

[26] Wang TS, Yang J, Shang CJ, Li XY, Lv B, Zhang M, Zhang FC. Sliding friction surface microstructure and wear resistance of 9SiCr steel with low-temperature austempering treatment. Surface and Coatings Technology. 2008 May 15;202(16):4036-40.

[27] Zhang P, Zhang FC, Yan ZG, Wang TS, Qian LH. Wear property of low-temperature bainite in the surface layer of a carburized low carbon steel. Wear. 2011 Jun 22;271(5-6):697-704.

[28] Yang J, Wang TS, Zhang B, Zhang FC. Sliding wear resistance and worn surface microstructure of nanostructured bainitic steel. Wear. 2012 Apr 5;282:81-4.

[29] Vuorinen E, David PI, Lundmark J, Prakash B. Wear characteristic of surface hardened ausferritic Si-steel. Journal of Iron and Steel Research, International. 2007 Sep 1;14(5):245-8.

[30] Bakshi SD, Leiro A, Prakash B, Bhadeshia HK. Dry rolling/sliding wear of nanostructured bainite. Wear. 2014 Aug 15;316(1-2):70-8.

[31] Rementeria R, García I, Aranda MM, Caballero FG. Reciprocating-sliding wear behavior of nanostructured and ultra-fine high-silicon bainitic steels. Wear. 2015 Sep 15;338:202-9.

[32] Leiro A, Kankanala A, Vuorinen E, Prakash B. Tribological behaviour of carbide-free bainitic steel under dry rolling/sliding conditions. Wear. 2011 Nov 1;273(1):2-8.

[33] Leiro A, Vuorinen E, Sundin KG, Prakash B, Sourmail T, Smanio V, Caballero FG, Garcia-Mateo C, Elvira R. Wear of nano-structured carbide-free bainitic steels under dry rolling–sliding conditions. Wear. 2013 Feb 15;298:42-7.

[34] Yang HS, Bhadeshia HK. Austenite grain size and the martensite-start temperature. Scripta materialia. 2009 Apr 1;60(7):493-5.

[35] Talonen J, Hänninen H. Formation of shear bands and strain-induced martensite during plastic deformation of metastable austenitic stainless steels. Acta materialia. 2007 Oct 1;55(18):6108-18.